FLOW REVERSAL IN TURBULENT MIXED CONVECTION IN VERTICAL PIPE

A FLOW REVERSAL STUDY IN OPPOSING FREE AND FORCED CONVECTIVE FLOW IN A VERTICAL TUBE

By

BRIAN KA-HUNG TSANG, B.ENG.

A Project Report
Submitted to the School of Graduate Studies
in Partial Fulfilment of the Requirements
for the Degree
Master of Engineering

McMaster University
December 1975

MASTER OF ENGINEERING (1975) McMASTER UNIVERSITY
(Chemical Engineering) Hamilton, Ontario

TITLE: A Flow Reversal Study in Opposing Free and Forced Convective Flow in a Vertical Tube

AUTHOR: Brian Ka-Hung Tsang, B. Eng.,
(McMaster University)

SUPERVISOR: Dr. T. W. Hoffman

NUMBER OF PAGES: viii, 81

ABSTRACT

Flow reversal conditions in the turbulent opposing convection regime were investigated in the cooling of upflow water and the data correlated by the equation:

$$\frac{Gr}{Re^{2.58}} = \frac{0.053}{Pr}$$

for $6 \leq (\frac{L}{d}) \leq 18$. The Metais-Eckert plot, which depicts the region of natural/forced convection interaction effects on the heat transfer coefficient, was found to be unsuitable for correlating the conditions for which flow reversal occurs because of the improper inclusion of the parameter $(\frac{d}{L})$.

ACKNOWLEDGEMENT

The author would like to express his sincere gratitude to:

His research supervisor, Dr. T. W. Hoffman, for his guidance, advice and encouragement throughout this work.

R. W. Dunn and J. J. Newton, for their help in the fabrication of the experimental equipment.

TABLE OF CONTENTS

.....Cont'd

LIST OF ILLUSTRATIONS

.....Cont'd

LIST OF TABLES

CHAPTER 1

INTRODUCTION

Combined free and forced convection plays a very important part in heat transfer processes such as reactor coolant circulation and gas/liquid cooled turbines. Although considerable research work has been directed to obtaining heat transfer coefficients in cases of aiding and opposing convection situations, very few studies have been done in the turbulent mixed convection region. Metais[14] attempted to map free, forced, and mixed convection regimes in laminar and turbulent flow; however, most of the data he used were from aiding flow conditions. Eckert et.al.[4] found that in the case of aiding turbulent mixed convection McAdam 's rule can be used as a good first approximation to obtain the corresponding heat transfer coefficients. However the same rule when applied to opposing turbulent mixed convection gave heat transfer rates as much as 50% lower than the experimental value, which suggests that aiding and opposing mixed convections are two hydrodynamically different processes. Khosla[3] experimented with opposing mixed convection air flow in the unidirectional flow region. To delineate the experimental conditions over which unidirectional flow existed, it was necessary for him to identify the flow reversal conditions as his lower operating limit. However, only a small number of data points were obtained for this purpose, and one test section was employed in his work.

Thus the objective of this project is to identify the

conditions under which flow reversal occurs in various opposing mixed convection situations, and to investigate the dependence of this phenomena on the diameter and length of the heat transfer section. In addition, the data thus obtained could be used to check the applicability of Metais' tentative plot for turbulent opposing flow systems.

CHAPTER 2

LITERATURE REVIEW

2.1 Introduction

For the past six decades, considerable experimental and theoretical work has been done on various aspects of combined free and forced convection heat transfer; however few of them actually focused on the identification of conditions for flow reversal in opposing convections, especially in the turbulent mixed regime.

Although flow reversal can occur in aiding as well as opposing situations, one must distinguish between the two cases. In aiding flow, the fluid at the wall is accelerated to such an extent that there is more flow at the wall than can be accomodated by the inlet flow, thus causing the flow to reverse at the centre-line of the tube. The transition to unstable flow is gradual through the growth of small disturbances, and it requires a longer heat transfer section for reversal to occur.

In the case of opposing flows, the reversal takes place next to the wall; it is associated with separation at the wall, and occurs suddenly as observed by Scheele and Hanratty[1]. Also, over the same turbulent Reynolds range, Herbert and Sterns[2] found that the heat transfer coefficient for aiding flow is 50% lower, and for opposing flow 36% higher, than those predicted by Dittus-Boelter equation. Similarly, in the heating of turbulent downflow air, Khosla[3] observed that the heat

transfer coefficient was increased by as much as 215% near the flow reversal point. Earlier work by Eckert et.al.[4] using a short vertical tube of L/d = 5 also gave decreased heat transfer when the forced flow was in the same direction as the free flow, and increased heat transfer when it opposed the free flow. In a different experiment by Thomas[5], similar observations were obtained in the case of laminar opposing flows.

The purpose of this review, then, is to identify:

(i) the important factors affecting opposing flows,
(ii) the effect of reversal on heat transfer rates,
(iii) previous work done on this specific topic, and
(iv) the various techniques employed for flow visualization.

2.2 Factors affecting opposing flows

2.2.1 Physical property variation

Flow reversal in opposing flow can be obtained by the cooling of upflow, or heating of downflow fluid. The two processes are hydrodynamically similar but the physical property variation with temperature may cause differences to be observed.

The physical properties which can vary and have a measurable effect are density, thermal conductivity, heat capacity and viscosity. In the cooling of upflow water, heat capacity and thermal conductivity stay relatively constant, and density and viscosity affect the velocity profile. If

only the fluid density varies, the steady state velocity and temperature fields eventually become invariant with heat transfer length; if however viscosity variation is also significant, the steady state temperature and velocity profiles will never attain invariant form[6]. Variable thermal conductivity affects both temperature and velocity profiles but to a lesser degree.

In his theoretical analysis, Pinkel[7] found that at moderately high temperatures, systematic deviation from the constant property solution can be observed even at high Reynolds numbers, indicating the effect of physical property variation. However, if the physical properties are evaluated at some film temperature, i.e. some average between the wall and bulk temperature, the effect of variable properties can be partially eliminated[8]. Therefore, in analyzing experimental results it is important that an appropriate averaging method be employed for the particular fluid used, and it should be applicable over the full range of experimental conditions.

2.2.2 Relaminarization

When turbulently upflowing water is cooled in a pipe with high coolant flow, its viscosity in the wall region increases. Since turbulence is generated in the wall region, the increased viscosity is expected to dampen the fluid turbulence. Indeed, if the heat exchanger is long enough, under

some conditions it may be possible to reduce the Reynolds number of the flow sufficiently that it reverts to laminar flow. In any event, the transport processes in the wall region should be affected by this damping effect.

Hall and Jackson[9] also reported that relaminarization can occur under favourable pressure gradients arising in strongly accelerating flow; this leads to a reduction of the shear stress level in the wall region and thus diminishes turbulence production. However, this effect is expected to be much more important in the high temperature heating of gases rather than the intermediate temperature range encountered in the cooling of upflow water.

2.2.3 Turbulent eddy quantities

It is well known that in near isothermal flow, the rates of transfer of heat and momentum between a solid wall and a fluid in turbulent flow near a wall can be characterized by an eddy diffusion coefficient, namely eddy diffusivity for heat (ε_h) and eddy viscosity for momentum (ε).

In isothermal flow, that is in the absence of buoyancy forces, the total shear associated with the transport of momentum in the direction normal to the wall is given by

$$\tau g_c = \mu \frac{\partial \bar{u}}{\partial y} - \overline{\rho v' u'} \qquad (2.1)$$

The term $\overline{\rho v'u'}$ thus corresponds to the turbulent contribution and may be expressed as

$$\overline{\rho v'u'} = \rho\varepsilon\frac{\partial \bar{u}}{\partial y} \tag{2.2}$$

which can be taken as a definition of eddy viscosity. Prandtl further correlated the turbulent shear stress and eddy viscosity with the mixing length concept. In addition, he hypothesized that mixing length is proportional to distance from the wall, which resulted in the relations

$$\varepsilon = \ell^2 \frac{du}{dy} = k^2 y^2 \left|\frac{du}{dy}\right| \quad . \tag{2.3}$$

Van Driest[10] later modified the mixing length to

$$\ell = ky\{1 - \exp(-y/A)\} \tag{2.4}$$

to include the damping effect of the wall region on mixing.

The equations are usually expressed in dimensionless quantities defined as:

$$y^+ = \frac{\rho u^* y}{\mu} \quad , \quad u^+ = \frac{u}{u^*} \quad , \quad \text{and} \quad \varepsilon^+ = \frac{\varepsilon}{\upsilon} \tag{2.5}$$

where

$$u^* = (\tau_w/\rho)^{\frac{1}{2}} \quad . \tag{2.6}$$

Since then, many turbulent exchange models have been proposed by various authors for the eddy viscosity for momentum transfer[11]. These expressions were obtained for fully developed iso-

thermal flow and these have a built-in assumption of a linear variation in shear stress over the pipe cross-section. However, Khosla[3] observed that the shear stress profile is influenced by the buoyancy force if the latter is of comparable magnitude. The shear stress at the wall is greatly reduced because the greatest buoyancy force occurs there. In fact, under some conditions, the shear stress may become zero and then negative if flow reversal occurs. Thus the shear stress variation with radius is far from linear in the presence of opposing convection. As a result, the applicability of such expressions in the present experimental conditions is questionable.

The eddy diffusivity for heat is usually assumed to be proportional to eddy viscosity with the proportionality constant known as the turbulent Prandtl number,

$$Pr_t = \frac{\varepsilon}{\varepsilon_h} \quad . \qquad (2.7)$$

By the Reynold's analogy $Pr_t=1$, which says that the mixing length for momentum is identical to the mixing length for heat. Bourne[12] examined the validity of such an assumption and concluded that it should be used with considerable care. Quarmby[13] suggested the modification based on available experimental data, viz:

$$Pr_t = \{1 + 400^{(R-1)}\}^{-1} \quad . \qquad (2.8)$$

This expression was determined by a regression analysis of the available experimental data; it exhibits considerable scatter of $\pm$15% around it. In addition, Khosla[3] observed a systematic increase in ε_h with (Gr/Re^2), indicating that with the increase in the interaction between free and forced convection the contribution of the turbulent transport of heat increases. This effect is not taken into account at all by the formulae for Pr_t.

2.3 Mapping of free, mixed and forced convections

Since the heat transfer coefficient varies greatly for laminar and turbulent flow, natural(free) and forced flow(either aiding or opposing), it is desirable to have available a generalized mapping of the purely forced or free convective regions(that is, where one convective region does not affect the other) and that region where mixed convection has a significant effect on the heat transfer rate. Metais and Eckert[14] have attempted to define these various regions for vertical tubes by plotting the Reynolds number versus $GrPr\frac{d}{L}$ (Figure 1) and indicating those regions on this plot where the measured heat flux was greater than 10% of that predicted from pure forced convection or free convection correlations. Most of the data for the forced/natural convection interaction was from aiding flow situations; only few were from opposing flow. It does include data from both uniform wall temperature and uniform wall heat flux

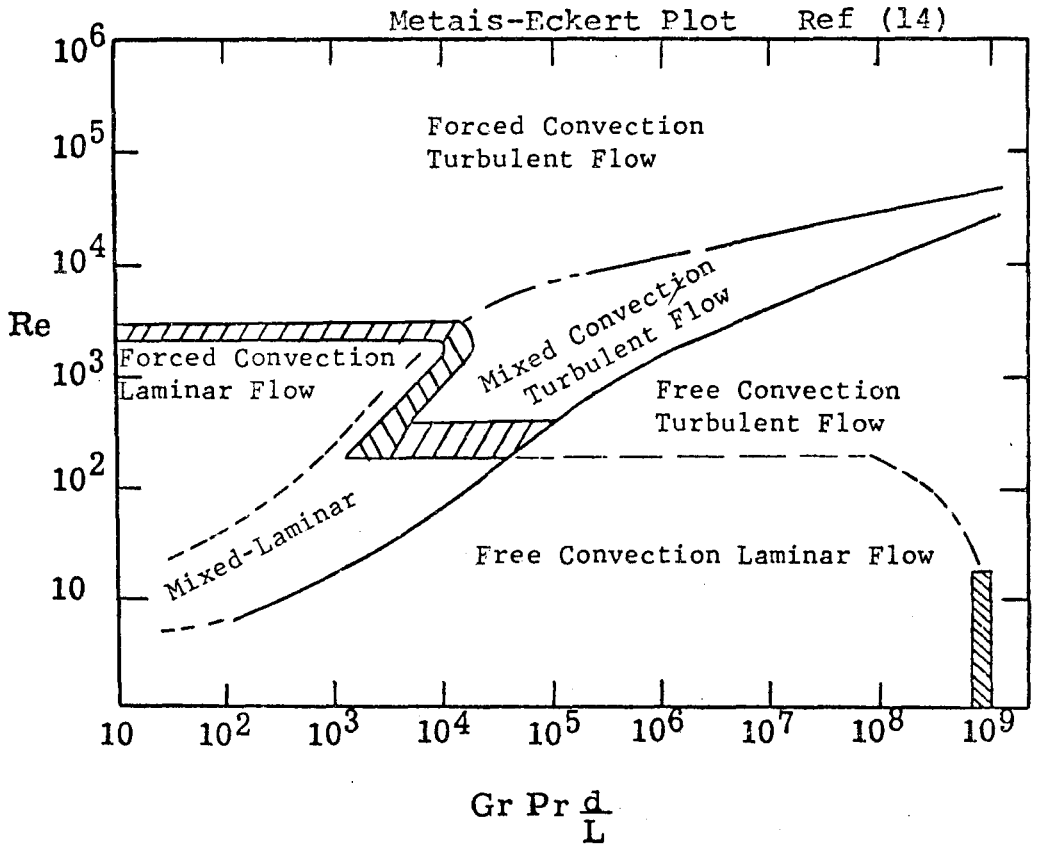

Fig 1. Regimes of free, forced, and mixed convection for flow through vertical tubes.

$$(10^{-2} < \Pr \frac{d}{L} < 1)$$

experiments. This mapping does not show the demarkation between uni-directional and reverse flow. Obviously if the mapping parameters are correct this reversal should occur in the mixed convection region.

2.4 Previous work on opposing convections

The results of only a few investigations on turbulent mixed opposing convection heat transfer and flow visualization are available. Most work has been done in the laminar region with emphasis on transition to unstable flow rather than the actual reversal of flow at the wall region. These results are included here for the sake of comparison. It should also be noted that in laminar opposing convection the ratio of buoyancy to viscous force (Gr/Re) is important, whereas in the case of turbulent opposing flow, the ratio of buoyancy to inertia forces (Gr/Re^2) is of greater interest.

2.4.1 Mixed laminar

Gensini[6] observed the downflow heating of a Newtonian fluid (5.15% by weight of polystyrene in xylene) in a 1 in. tube. The instability of the system was indicated by the change of symmetrical flow to asymmetrical flow, as indicated by the temperature profile, at critical (Gr/Re) of 58.1 to 76.6 for Re from 90 to 201 and $(\frac{L}{d})$ from 341 to 245. The instability was found to be associated with intermittent bursts of turbulence (as shown by photosensitive dye), interspersed with the laminar behaviour characteristic of flow separation;

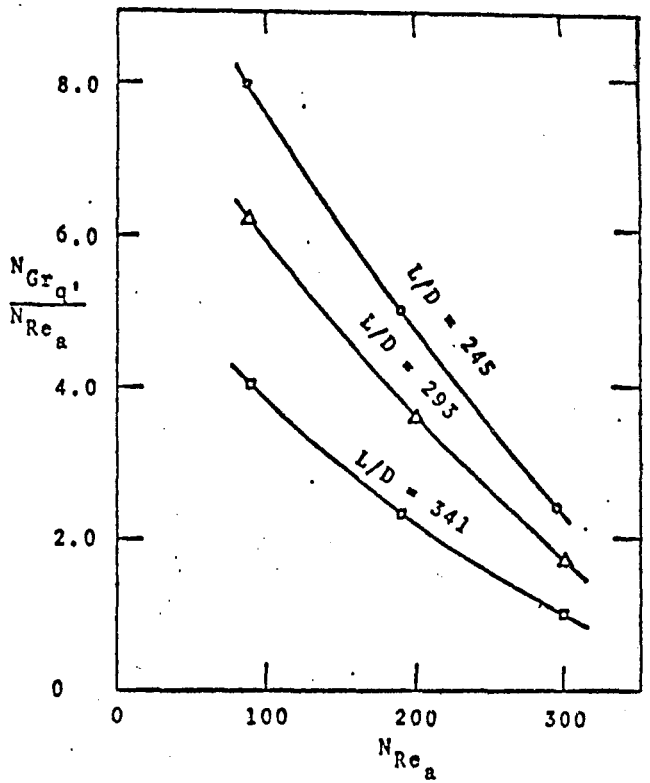

Fig 2. Transition to Asymmetric Temperature Profiles. Gensini. Ref (6).

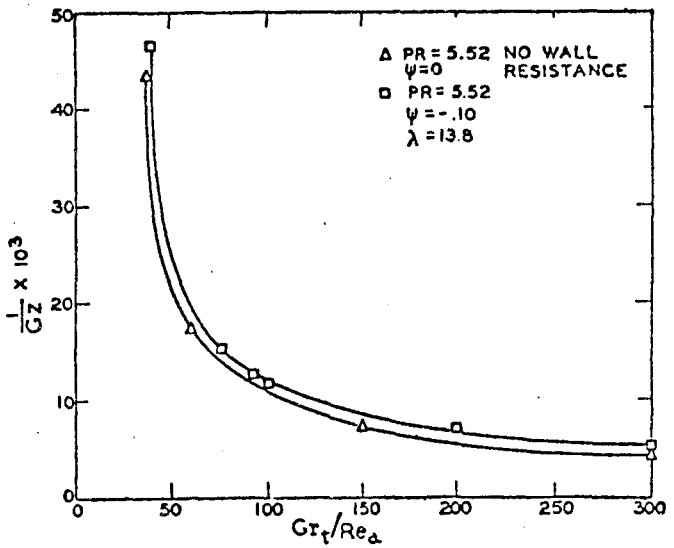

Fig 3. Location of zero velocity Gradient at Wall for Constant Temperature Cooling in Upflow. Scheele et.al. Ref(15).

however, no flow reversal was detected prior to occurrence of the bursts and reversal was delayed until (Gr/Re) exceeded 100. The $(\frac{L}{d})$ effect is shown in Figure 2.

Scheele, Rosen and Hanratty[15] observed both the downflow heating and upflow cooling of water in a 2.19 cm. I.D. Pyrex glass tube in the range of Re from 120 to 654 and $(\frac{L}{d})$ = 77.6. From theory, the transition to asymmetric flow and turbulence occurs at (Gr/Re) of 41.5 for upflow and 49.2 for downflow. The experimental values obtained were (Gr/Re) at 74 for upflow and 63 for downflow. It was not possible, however, to detect the transition point exactly because of the difficulty in visually detecting the onset of the first disturbance of the injected dye filament. The results obtained were also plotted as shown in Figure 3 and Figure 4.

Rosen[16] observed the cooling of upflow water in a 2.19 cm. I.D. glass tube with $(\frac{L}{d})$=83.3 using methylene blue dye. He observed that the centre-line velocity increases to a maximum and then decreases. The transition point being indicated by the breakup of dye at the centre-line. The critical (Gr/Re) thus obtained was at 58, 38, 38 respectively for Pr of 0.73, 5.52 and 50. He also reported difficulty in locating the breakup point which was time dependent.

Scheele and Hanratty[1] observed the downflow

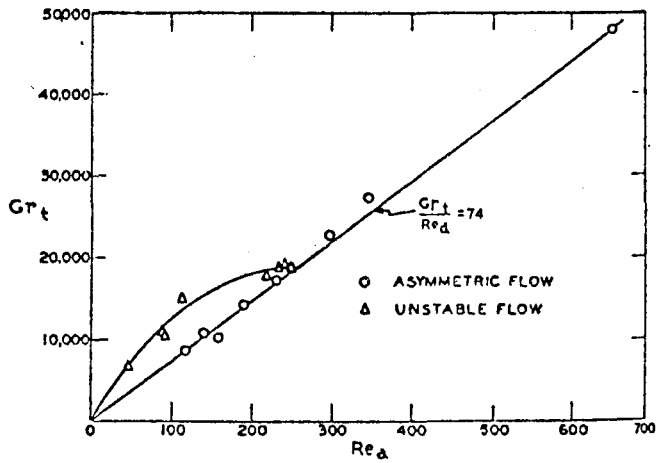

Fig 4. Transition to Asymmetric Flow for Upflow Cooling-Constant Wall Temperature. Scheele et. al. Ref (15).

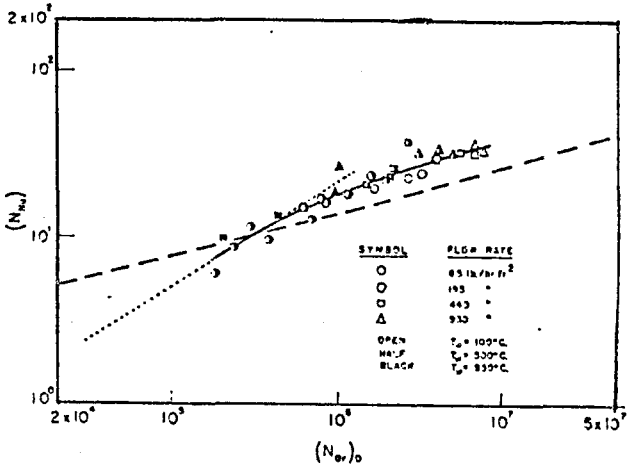

Fig 5. Heat Transfer Results in Turbulent Opposing Flow. Brown et.al. Ref (17).

heating of water in a 0.787 in. I.D. copper pipe for Re<1600. They also observed that transition to unsteady flow was preceded by asymmetry in the flow field, then transition was associated with flow reversal, and alternate separation and attachment of the fluid near the wall at high frequency. Also a sharp decrease in wall temperature was noted when the tail end of a turbulent burst passed a given location. Critical (Gr_q/Re) was established at values greater than 52.2 for all values of Re<1600.

2.4.2 Mixed turbulent

Brown and Gauvin[17] investigated the heat transfer rate in fully developed opposing turbulent convection in heating of downflow air in a 4.42 in. I.D. tube, 101.5 in. long, in the Re range of 380 to 6900, Gr from 0.18×10^6 to 7.3×10^6, and $(\frac{L}{d})$ from 5.43 to 13.6. Their results are shown in Figure 5. The dashed line represents pure free convection. These results indicated that the laminar opposing convection heat transfer rate is lower, and the turbulent opposing convection heat transfer is 45% higher, than that calculated for pure free convection. The explanation put forward is that in opposed flow, the buoyancy force acts in a direction such that the velocity gradient at the wall should be reduced, thus reducing the heat transfer rate, as observed in the laminar case. However, as the Grashof number increases, the inter-

action of increasing buoyancy forces and the force flow generates turbulence, thus increasing the rate of heat transfer above the expected value.

Herbert and Sterns[2] experimented with heating water in a 0.901 in. I.D. copper pipe of $(\frac{L}{d}) = 80$. They reported that at Re<18,000 , a marked increase heat transfer rate occurs if cold water is caused to flow downwards through heated tubes rather than upwards. Under downflow conditions they obtained film coefficients up to 2.3 times greater than those in upward flow at Re = 15,000. Also in downflow heating, heat transfer coefficients were up to 36% higher than those predicted by the Dittus-Boelter correlation at Reynolds number below about 12,000. In upflow, the coefficients were measured to be constant low values (at Re≈15,000) and were approximately half of the Dittus-Boelter predicted values.

Hall and Price[18] also found that opposing free and forced convection increases heat transfer data as opposed to laminar mixed convection in the heating of air by a hot vertical plate.

Khosla[3], using the same equipment as the present author, experimented with the cooling of upflow water in a 3 in. pipe of $(\frac{L}{d}) = 12$. The flow reversal was observed with thymol blue pH indicator, which will be described in detail later in this report. The data he obtained are plotted on the Metais-Eckert plot as shown in Figure 6.

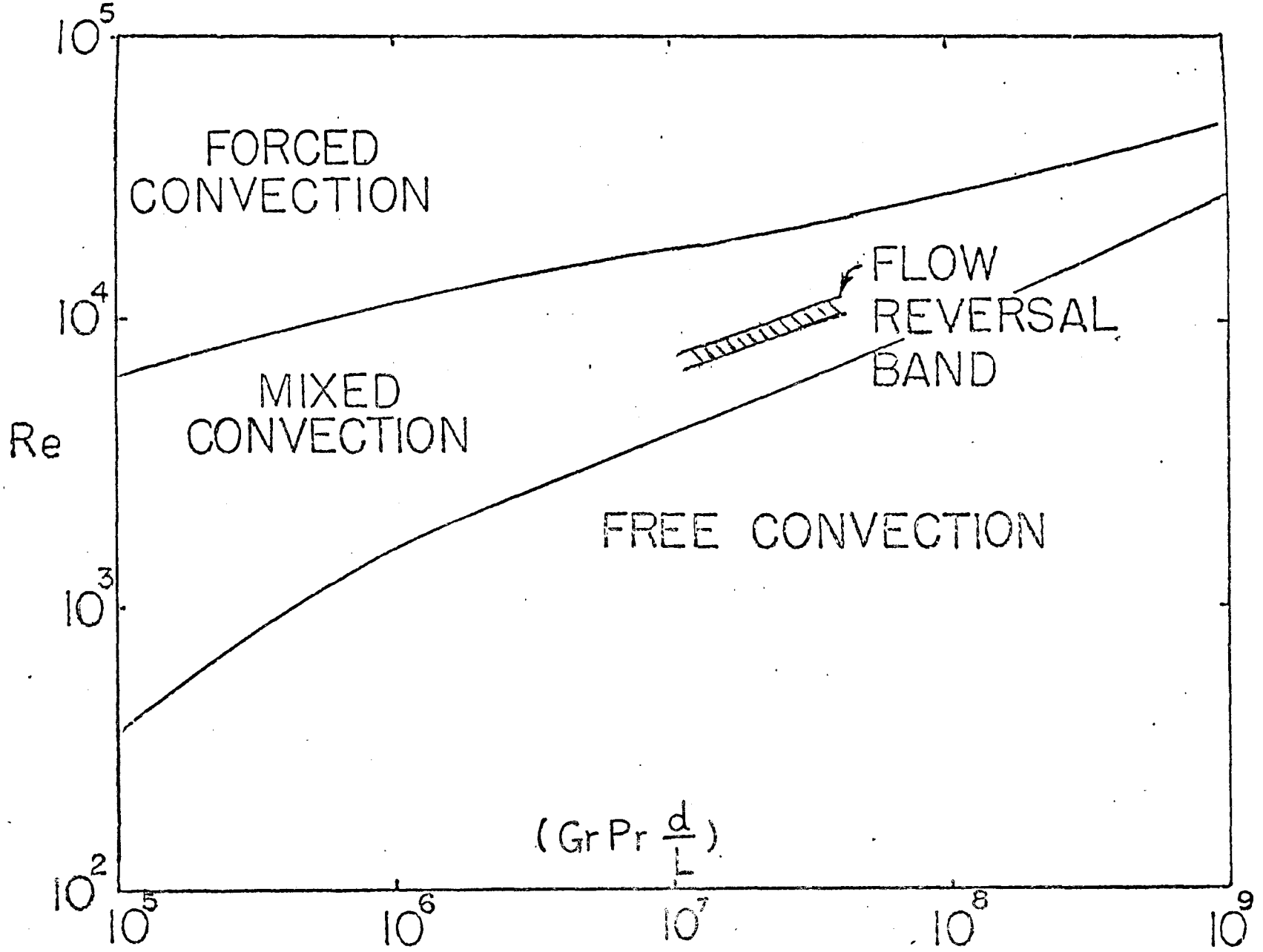

Fig 6. The Band Representing the Initiation of Flow Reversal in Opposing Free and Forced Convection. Khosla. Ref (3).

Two experimental points indicating flow reversal in the downflow heating of air in a 8 in. diameter tube of $(\frac{L}{d})$ = 3 agreed with the results of the upflow cooling of water.

2.5 Visualization techniques

Gensini[6] used photochromic spiropyran, (or 1,3,3,-trimethylindoline-6'-nitrobenzopyrylospiran), as an indicator in flow visualization experiments to detect the transition from symmetric to asymmetric flow.

In their experiments on the stability of flow, Hanratty, Rosen and Kabel[19] used direct injection of methylene blue dye into the centre-line of the tube by hypodermic needle.

Sherwood, Smith and Fowle[20] used dark background multiple exposure microphotography of minute tracer (1μ diameter iron particles) to measure the velocity profile.

Hummel and Popovich[21] employed 2-(2,4-dinitrobenzyl)-pyridine in 95% ethyl alcohol which gives a blue trace when exposed to high intensity light, emitted from a parabolic mirror, to measure velocity profiles and turbulence characteristics.

Khosla[3] used the pH sensitive thymol blue sodium salt solution which changes colour in the pH range of 8.0 - 9.2 from yellow to dark blue at the cathode to indicate flow reversal. This flow visualization technique was first suggested by Baker[22].

CHAPTER 3

SOLUTION OF THE CONSERVATION EQUATIONS FOR MIXED CONVECTION

3.1 Theoretical analysis

Theoretical analysis of combined free and forced convection for flow through a vertical pipe has been described in great detail in the Ph.D. thesis of Khosla [3]; therefore, only the main points will be mentioned here.

The equations to be solved are:

(i) Continuity

$$\frac{\partial}{\partial x}(\rho u) + \frac{1}{r}\frac{\partial}{\partial r}(\rho v r) = 0 \qquad (3.1)$$

(ii) Conservation of mass

$$2\pi \int_{o}^{R_o} ur\rho dr = \text{Total mass flowrate} \qquad (3.2)$$

(iii) Conservation of momentum

$$\rho u\frac{\partial u}{\partial x} + \rho v\frac{\partial u}{\partial r} = -g_c\frac{dP}{dx} + \frac{1}{r}\frac{\partial}{\partial r}\{r(\mu+\varepsilon\rho)\frac{\partial u}{\partial r}\} - g_c(\rho-\rho_o) \qquad (3.3)$$

(iv) Conservation of energy

$$\rho u\frac{\partial T}{\partial x} + \rho v\frac{\partial T}{\partial r} = \frac{1}{r}\frac{\partial}{\partial r}\{r(\frac{k}{C_p} + \varepsilon_h\rho)\frac{\partial T}{\partial r}\} \qquad (3.4)$$

The simplifying assumptions are:

(i) Two-dimensional steady-state, unidirectional, axi-

symmetric flow prevails.

(ii) The magnitude of the radial pressure gradient is small so that only the axial momentum conservation equation needs to be considered.

(iii) Time-averaged values of the fluctuating components of the axial and radial velocity and of temperature are zero, so that the conservation equations are fully described by the time-averaged values of the velocities and temperatures.

(iv) Axial diffusion of momentum and energy can be neglected in comparison with radial diffusion.

(v) Viscous dissipation is negligible and the flow is incompressible.

(vi) Effective momentum and thermal diffusivities are sums of molecular and turbulent diffusivities, that is, the molecular and turbulent transport processes are additive.

(vii) Equilibrium between generation, dissipation, advection and diffusion of turbulent kinetic energy is assumed such that flow similarity conditions prevail and the turbulent eddy diffusivity is a function of radial position only.

(viii) Eddy diffusivity is calculated from the empirical equations available in the literature for isothermal turbulent flow.

(ix) The flow field does not contain any heat source.

On non-dimensionalizing using variables defined as:

$$X=\frac{x}{R_o}\ ,\quad R=\frac{r}{R_o}\ ,\quad RO=\frac{\rho}{\rho_o}\ ,\quad U=\frac{u}{\bar{u}_o}\ ,\quad V=\frac{v}{\bar{u}_o}\ ,$$

$$P=\frac{pg_c}{\rho_o \bar{u}_o^2}\ ,\quad Re_o=\frac{R_o \bar{u}_o \rho_o}{\mu_o}\ ,\quad \theta=\frac{T-T_o}{T_w-T_o} \tag{3.5}$$

and

$$Gm = (\mu + \varepsilon\rho)/\mu_o \tag{3.6}$$

$$Gh = \left(\frac{k}{C_p} + \varepsilon_h \rho\right)/\mu_o \tag{3.7}$$

where R_o is the radius of the pipe and the subscript o is used to indicate the inlet conditions. The dimensionless forms of the continuity, conservation of mass, momentum and energy equations become:

(i) $$\int_o^1 (RO)\,UR\,dR = 1/2 \tag{3.8}$$

(ii) $$\frac{\partial}{\partial X}\{(RO)U\} + \frac{1}{R}\frac{\partial}{\partial R}\{(RO)RV\} = 0 \tag{3.9}$$

(iii) $$(RO)U\frac{\partial U}{\partial X} + (RO)V\frac{\partial U}{\partial R} = -\frac{dP}{dX} + \frac{1}{Re_o}\frac{1}{R}\frac{\partial}{\partial R}\left(RGm\frac{\partial U}{\partial R}\right) - \frac{R_o g_c}{\rho_o \bar{u}_o^2}(\rho-\rho_o) \tag{3.10}$$

(iv) $$U\frac{\partial \theta}{\partial X} + (RO)V\frac{\partial \theta}{\partial R} = \frac{1}{Re_o}\frac{1}{R}\frac{\partial}{\partial R}\left(RGh\frac{\partial \theta}{\partial R}\right) \tag{3.11}$$

The appropriate boundary conditions are:

1. Fully developed (or known) inlet velocity profile $U(0,R) = U(R)$.
2. Uniform inlet temperature profile $\theta(0,R) = 0$.
3. Uniform (or known) wall temperature distribution

$\theta(X,1) = 1.$

4. No slip, suction or blowing at the wall $U(X,1) = V(X,1) = 0.$

5. Axi-symmetric velocity profile $\left.\frac{\partial U}{\partial R}\right|_{R=0} = 0.$

6. Axi-symmetric temperature profile $\left.\frac{\partial \theta}{\partial R}\right|_{R=0} = 0.$

7. The diffusive transport of momentum term in equation (3.10) at the centre-line becomes

$$\left.\frac{1}{R}\frac{\partial}{\partial R}\left(RGm\frac{\partial U}{\partial R}\right)\right|_{R=0} = 2Gm\frac{\partial^2 U}{\partial R^2} \qquad (3.12)$$

by L'Hospital's Rule.

8. Similarly the diffusive transport of heat term in equation (3.11) at the centre-line becomes

$$\left.\frac{1}{R}\frac{\partial}{\partial R}\left(RGh\frac{\partial \theta}{\partial R}\right)\right|_{R=0} = 2Gh\frac{\partial^2 \theta}{\partial R^2} \qquad (3.13)$$

by L'Hospital's Rule.

The above equations have been solved by the combination of Crank-Nicholson, central difference, finite-difference formulations using an implicit scheme. In the present case of a developing thermal boundary layer, the gradients near the wall and at the start of the heat transfer section are likely to be very large; thus a fine mesh size is required at these locations and the mesh size increases as one leaves the region of maximum changes. This was accomplished by the use of the following variable grid spacing formula,

$$\Delta_k = \frac{H^k - 1}{\sum_{k-1}^{N-1} (H^k - 1)} \qquad k=1,2,3,\ldots,N-1. \qquad (3.14)$$

where N is the number of nodes along any of the axes and H is a constant greater than 1. The fineness of the mesh increases with the value of H. In this case H=1.05 was used for both the radial and axial directions. Thus for the radial direction, at the centre-line, i=1 and $R_i=0$; at other nodes $i\geq 2$, $R_i = R_{i-1} + \Delta_{N-i+1}$. For the axial direction, at the start of heat transfer section, j=1 and $X_j=0$; at other nodes $j\geq 2$, $X_j = X_{j-1} + L.\Delta_j$ where L is the maximum number of radii to be travelled in the axial direction. A Fortran program was written by Khosla to solve the set of numerical equations, the solution of which was successfully tested in cases of isothermal laminar and turbulent flow.

3.2 Finite difference solution of the set of conservation equations

Since the original program was written for the case of combined free and forced convection in the heating of air flowing downward through a vertical tube of constant wall temperature, it was necessary, in order to apply it to the present case of cooling of water flowing up a vertical tube, to replace the appropriate physical properties of water for those for air. This involved expressing the density, viscosity, thermal conductivity, and specific heat of water as functions of temperature, as listed in Appendix D-1.

In the actual simulation of the experimental system, the program would:

(i) start with a flat velocity profile at a given temperature at the bottom of the developing section,

(ii) develop an isothermal velocity profile for a distance of eleven feet which would take the fluid to the entrance of the heat transfer section.

(iii) for a given length of test section and a given inside wall temperature (established from experimental data), the program would develop the velocity and temperature profiles as the fluid progresses up through the test section until the velocity of the fluid at some radial mesh point just becomes negative, at which point the computer program would stop executing. This corresponds to the point of flow reversal which should be observed in the actual experiment if all assumptions in the original formulation are valid.

The difficulty encountered here was that of obtaining a reversal profile right at the end of a given length corresponding to the actual experimental test section for given fluid and wall temperatures. This could only be done by trial and error and involved obtaining the full solution at various mass flowrates of hot water into the heat transfer section, until flow reversal was observed at the exit of a given test section under a given temperature conditions. This approach was both time-consuming and expensive. The computation time was later reduced by decreasing the number of mesh points. As a result, only a limited number of cases were investigated. These were designed to provide the maximum amount of information on the limiting flowrate for reversal, such as:

(i) the effect of varying the length of the heat transfer section,

(ii) the effect of varying the tube diameter, and

(iii) the effect of changing the fluid and wall temperature.

The results thus obtained are shown in the following table:

			CONDITIONS AT FLOW REVERSAL			
RUN	D(in.)	L(ft.)	wall T(^{o}F)	fluid T(^{o}F)	Re	$GrPr(\frac{d}{L})$
1	4	3	116	138	16,766	8×10^{7}
2	4	2	116	138	16,370	1.2×10^{8}
3	3	3	116	138	11,916	2.5×10^{7}
4	4	3	90	106	12,003	3.5×10^{7}

TABLE 1 - THEORETICAL ANALYSIS

The above results were also plotted as shown in Figure 10 (page 46). It is noted again that in obtaining the above results the following important assumptions were made:

(i) the isothermal eddy diffusivities were applicable in non-isothermal situations.

(ii) $Pr_t = 1$.

Although these assumptions have been found to be invalid in systems with large buoyancy forces (discussed in section 2.2.3), they were used here, since more representative correlations are not available. Hence the

results of this theoretical investigation may not be applicable.

Also, by means of an iterative procedure, an attempt was made to evaluate the eddy diffusivity from isothermal correlations using the local shear stress values corrected for buoyancy instead of the wall shear stress. The solution failed to converge, however, because of instability problems thus introduced. This is not surprising because the original formalae were not derived on the basis of local shear stresses.

CHAPTER 4

EXPERIMENTAL SYSTEM

The experimental system for opposing natural-forced convective flow is shown diagrammatically in Figure 7. Basically it consists of a transparent acrylic test section through which hot water, in fully developed flow, travels upwards. The walls of this test section are kept cold by cooling water flowing in a similar transparent jacket. At any given temperature of the hot water, the hot water flow-rate is adjusted downward until flow reversal just occurs as indicated by a dye tracer at the wall. The flow reversal occurs at the wall because the highest buoyancy forces are located there.

Since the reversal point is best detected visually, a dye technique is required. The limitations on the dye are that it must be neutrally buoyant so that it will not affect the temperature and velocity fields, that it should be generated at the wall where the reversal takes place, and that it should be used in small quantity so as not to affect the physical properties of the bulk fluid.

4.1 Dye tracer technique

The tracer technique that best satisfies the above mentioned requirements is the electrochemical method suggested by Baker[22]. This method involves the reduction of hydrogen ion concentration at a platinum electrode (supplied from a D.C. voltage source) and the use of thymol blue as an indicator for detecting the

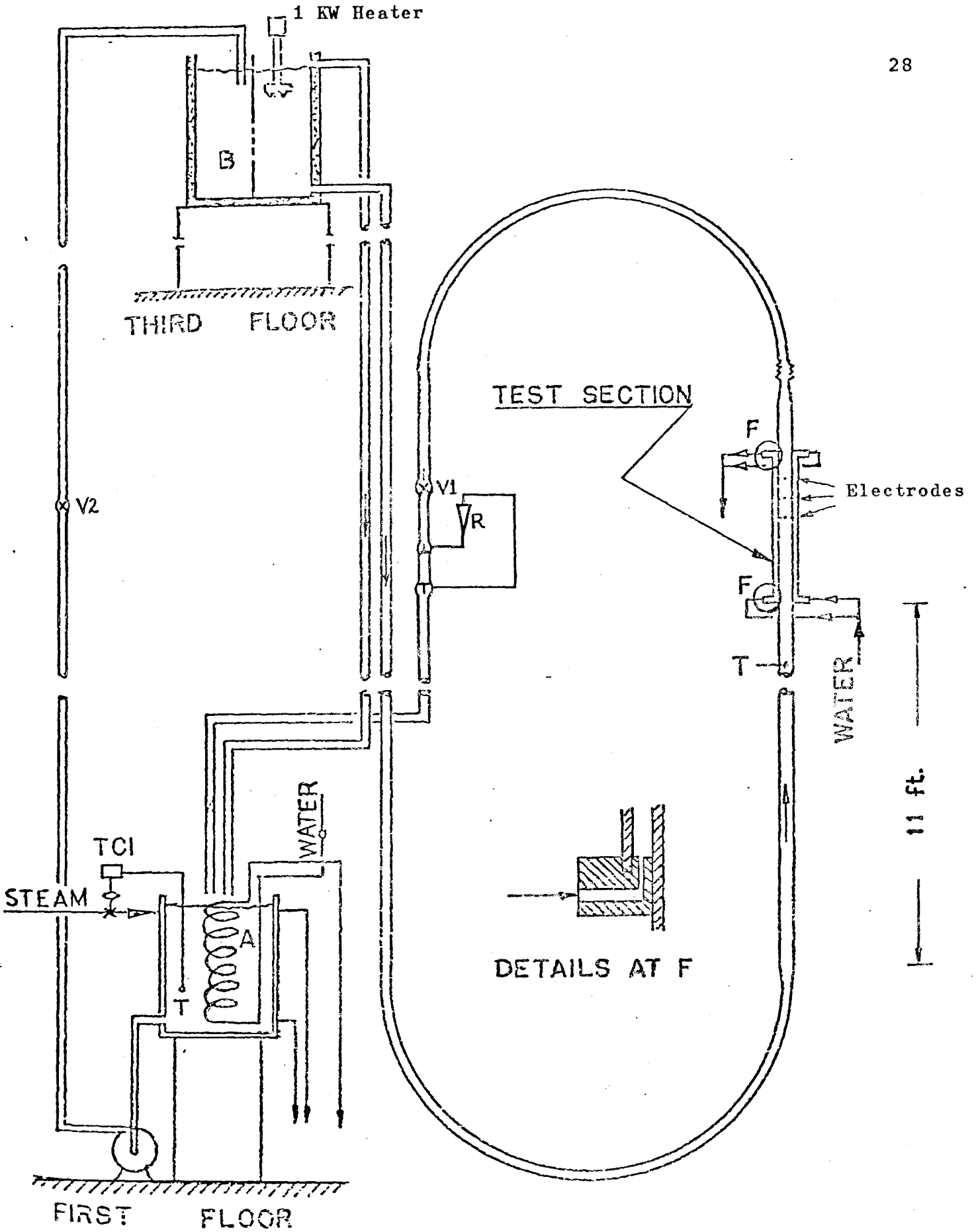

Figure 7 Experimental loop for Flow Reversal Study

hydrogen ion concentration changes. The sodium salt of thymol blue is preferred since it gives a distinct colour change from yellow to dark blue in the pH range of 8.0 - 9.2. The mechanism is that , at the end point

$$I^-_{yellow} \rightleftarrows I^=_{blue} + H^+ \qquad (4.1)$$

so that

$$K_2 = \frac{[I^=_{blue}][H^+]}{[I^-_{yellow}]} \qquad (4.2)$$

And at the cathode, the following reaction takes place:

$$H^+ + e^- \rightarrow H \qquad (4.3)$$ *

Therefore, at the cathode the hydrogen ion concentration $[H^+]$, decreases. To maintain K_2 constant, $[I^=_{blue}]$ has to increase, accompanied by a decrease in I^-_{yellow}, resulting in the observation of a blue dye emitting from the cathode.

The required concentration for a satisfactory colour response is 0.01% thymol blue by weight. Since the capacity of the whole system was estimated at 61.7 Imp. Gals. approximately, the amount of indicator needed was about 28 grams. Experiments showed that 5 grams of thymol blue salt when dissolved in 50 ml of N/200 sodium hydroxide solution required about 500 ml of N/10 hydrochloric acid to bring it to the yellow side of the end point when mixing was done in the system. This also provided a solution with sufficient electrical conductance. The impressed D.C. voltage required was from 16

*See Appendix F for structural changes.

to 20 volts for which the current was approximately 5 to 8 mA, depending on the distance between electrodes and the conductivity of the solution.

4.2 System as a whole

The complete system as shown schematically in Figure 7 consisted of a circulation loop fed from a 25 gallon constant head tank B, a 25 gallon heating tank A, a centrifugal pump, a flow developing section, a test section, and a flow control and measuring system.

Water was heated in tank A by a steam jacket and at the same time cooled by a copper cooling coil for better control of the water temperature. A thermocouple, an electro-pneumatic temperature control system and a mixer were used to maintain a desired uniform water temperature. Water from tank A was pumped by the centrifugal pump (96 gal/min. capacity) to the constant head tank B. Valve V1 controls the amount of hot water going from tank B into the test section. At the same time, tank B was kept at a constant head by proper adjustment of valve V2. Should the upflow into tank B exceed the total downflow, flooding would occur. By simultaneous adjustment of V1 and V2, the tank B was maintained at constant overflow level and tank A at a constant level as well. It was possible to make these adjustments so that the system could be run for an indefinite period of time for any desired flow through the test section.

Except for the developing section, test section, and stainless steel expansion bellows, all pipes were made of 2 in. copper tube. The eleven feet developing

section and test section were made from acrylic plastic (lucite) pipe. The inside diameters of the test sections were 1¼, 2, 3 and 4 in. I.D. The transition from 2 in. copper tube to the developing section and test section to bellows was achieved by two copper cones each 8 in. long. The stainless steel bellows served to release stresses caused by the difference in thermal expansion of copper and acrylic pipes. All piping, except the test section, was covered with 1½ in. fiberglass insulation. A copper-constantan thermocouple was located at approximately six feet upstream from the test section to measure the hot water temperature.

4.3 Test section

Four pairs of test sections of four different diameters were made up for the experiment. Each section was a double pipe cocurrent heat exchanger. The inside pipes were of 1¼, 2, 3 and 4 in. I.D. by 1/8 in. wall, respectively. For the 1¼ in. I.D. acrylic pipe, two test sections of one and two foot length were made. For the 2, 3 and 4 in. I.D. pipes, two test sections of two and three foot length each were made for each diameter. Hot water flowing in the test section was cooled by the cold water in the annulus. The cold water entrance was designed to avoid cold spots in the following way. Water flowed into the lower acrylic flange through two ½ in. holes, and then through fourteen 0.04 in. diameter holes, uniformly spaced around the periphery, into the annulus surrounding the inner pipe carrying the hot water. The upper outlet flange is of the same design.

With a high cold water flow, the outer heat transfer surface was maintained at essentially the constant cold water temperature. At the high cooling water flowrates, very little temperature rise was observed in it. ($<1^{o}C$)

To determine the inner wall temperature, five pairs of thermocouples were mounted at various axial distances from the exit end as shown in Table 2. They were equally distributed around the periphery of the test section. To minimize conduction error, the thermocouple wires were mounted in slots milled into the outside of the inner acrylic pipe. Each thermocouple pair was fixed in the slot at desired depths as shown in Table 2 by filling the slots with acrylic cement ('TENSOL' cement No.7, ICI) which has essentially the same physical properties as the acrylic plastic. Thus the inner and outer wall temperature of the inner acrylic pipe could be determined by linear extrapolation of the two temperatures measured at two different depths. Twelve electrodes, four at each level, were located at various distance from the exit end as shown in Table 2. At each level, the four electrodes were arranged at right angles to its neighbour. Holes were drilled at these twelve locations and twelve acrylic plugs were made to house the electrodes (Figure 8). The electrode was made of a 1/16 in. diameter platinum rod, 1 in. long. The plug with electrode mounted was machined to the same curvature as the inner pipe, and the electrode was flush with the wall so that the acrylic pipe remained hydrodynamically smooth throughout.

TABLE 2 Thermocouple and Electrode Locations on The Test Sections

Test Section		Distance from Exit End (in.)							
Length (Ft)	I.D. (in)	Locations of five pairs of thermocouples					Locations of electrodes (four electrodes per level)		
1	1¼	1	3.5	6.5	9.5	11	2	5	8
2	1¼	1	4	8	12	18	2.5	6	10
2	2	1	4	8	12	18	2.5	6	10
2	3	1	4	8	12	18	2.5	6	10
2	4	1	4	8	12	18	2.5	6	10
3	2	1	6	12	18	27	3	9	15
3	4	1	6	12	18	27	3	9	15
Remarks		Five pairs arranged spirally around periphery and equally spaced. For each pair, thermocouple junctions are to be at 0.035 and 0.090 in. from inner surface approximately.					Four electrodes at 90° to each other, plugs milled to tube curvature.		

Vertical Section Through Electrode And Pipes

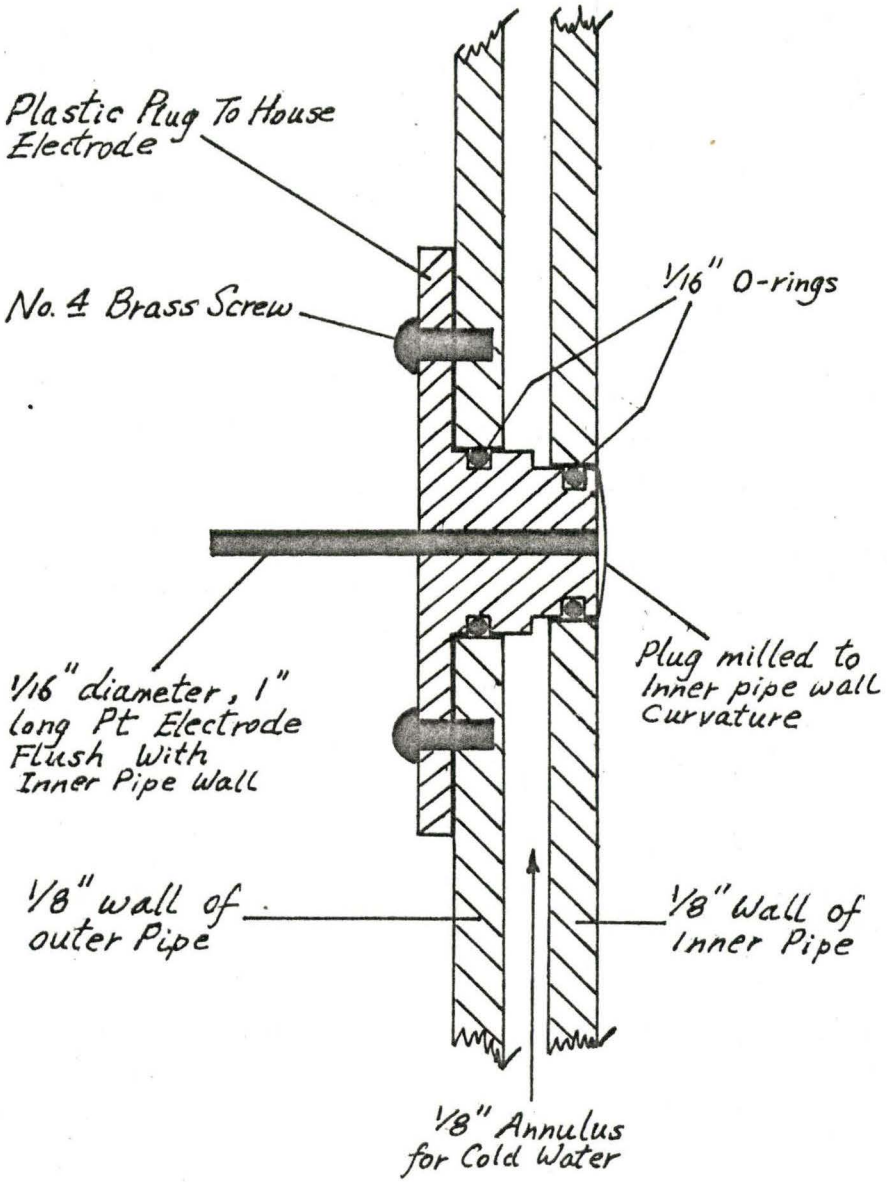

Sideview of Plastic Plug

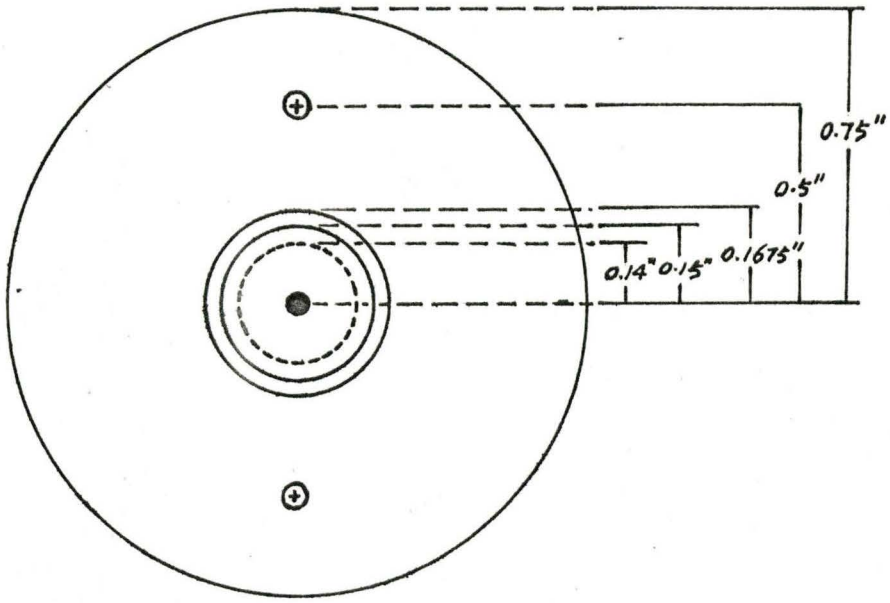

(Drawn to Scale Twice Actual Size)

Fig. 8 Electrode Design

4.4 Experimental procedure

4.4.1 Calibration of rotameters

The water to tank A was turned on, and the pump started. The water flowed to the system until a desired head was obtained in tank A and B and the circulation loop were filled. Rotameter R was calibrated by temporarily diverting the flow of water in the return leg of the loop into a barrel and weighing it. This procedure was repeated for other flowrates by manipulating valves V1 and V2 to vary the flow into the test section, without flooding or losing the head in tank B. Three different rotameters were used in the course of the experiment and their calibration curves are shown in Appendix E.

4.4.2 Instability experiments

The water in the circulation loop was heated to a predetermined temperature by supplying steam to the jacket of tank A and the cold water flowrate in the cooling coil was adjusted so that the steam valve remained partly open all the time to minimize temperature fluctuations. A one kilowatt tubular heating element was placed inside tank B to compensate for heat losses to the surroundings. The temperature of the water in the loop was controlled to better than $0.5^{\circ}F$ as observed by the thermocouple upstream of the test section. Cold water was supplied to the annulus of the test section at approximately 3 gpm. Five grams of thymol blue

sodium salt was then dissolved in 50 ml of N/200 sodium hydroxide solution in a beaker and then slowly added to tank A. This was repeated five times. The solution was dark blue in colour. Approximately 2.5 litre of N/10 hydrochloric acid was then added slowly to tank A. The time for the solution to change from dark blue to yellow depended mainly on the flowrate through the test section. Slightly more or less acid might be necessary to achieve the lightest yellow and yet keeping the pH close enough to the end point.

One of the twelve electrodes was then chosen as the cathode and the other eleven formed a common anode. A 22.5 volt D.C. dry battery was connected in series with a one kilo-ohm variable resistor to the electrodes. When the current was switched on, the hydrogen ion in the solution moved to the cathode, accepted an electron there to form hydrogen, and thus an increase of the local pH at the cathode resulted. The indicator would respond by changing from yellow to blue colour at the cathode, which appeared as a blue plume. The applied voltage was always kept at a minimum to reduce hydrogen bubble formation which could affect the flow pattern. When not in use, the circuit was switched off to conserve the battery.

The thermocouple for the hot water temperature and some of the thermocouples for wall temperature measurements were connected to a Honeywell chart recorder with a 0 - 5 mV span for visual

observation of the approach of steady state. When the temperature readings remained relatively constant, the circuit was switched on for flow visualization.

The point of instability was detected in the following way:

The hot water flowrate was adjusted to some high value so that essentially pure forced convection occurred. Under these conditions the dye would be flowing straight up along the tube wall. The hot water flowrate was then reduced by small amounts at a time until the dye slowed down and started to drift sideways. On further reducing the hot water flow, some of the blue dye at the wall would drift to locations below the electrode; this was a definite sign of reversal. The hot water flow was then increased slowly to reconfirm the flow range in which the reversal point took place. The accuracy of this method depends on the sensitivity of valve V2, the variability of the rotameter R, and the stability of the flow system at reversal.

Since the onset of reversal is not a clear-cut phenomenon, the flowrate at which reversal occurred was established by observing when a definite reversal occurred at most of the electrodes, while sideways drifting of the dye plume occurred at the others.

Change over to test sections of different

diameters involved the changing of the developing section, insulation and cones. For sections of 1¼ in. I.D. and 2 in. I.D. it was necessary to change the rotameter to accommodate the required flowrate at reversal. The experimental procedure for all test sections was the same. In addition, for each test section, runs were made for various hot water temperatures above 86°F up to the maximum of about 175°F. Above the maximum temperature there was a risk of deforming the acrylic pipe.

CHAPTER 5
EXPERIMENTAL DIFFICULTIES

The main difficulty experienced in this experimental program was in obtaining consistent wall temperature measurements. The wall temperature measurements at two different depths at essentially the same location were used to obtain the inner wall temperature by linear extrapolation, as described in Section 6.1.2. These extrapolations for a given test section under a given hot water condition resulted in considerable variability in the inner and outer wall temperatures. Since early difficulties were attributed to the use of fibreglass, cotton covered thermocouple wires, which seemed to draw cold water up the wires in the slot by strong capillary action, thus leading to very low temperature readings which did not change appreciably with the inner fluid temperature. This difficulty was overcome by using Kapton-insulated wires. The new wall temperatures still showed large and unnatural variations along the tube. In fact, in some instances the extrapolated inner wall temperature exceeded the hot fluid temperature. This suggested that the thermocouple junctions were not located at their prescribed depths. The only way to check this possibility was to destroy the test sections by cutting it and machining the test section until the thermocouple could be viewed directly at its actual location relative to the inside tube wall. This procedure did indicate a number of defects in the placing of the wall thermocouples. Not only were the locations relative to the tube wall different from those prescribed but

these observations also indicated other problems in mounting. These are summarized below:

(i) some thermocouple junctions were not located at the bottom of the milled slot,

(ii) the junction was located at the bottom of slot, but the slot was not completely filled with acrylic cement. In some cases, there were large voids around the thermocouple junction, leaving the junction in an air space; in other instances the slot was not completely filled, leaving a depression at the slot location. This effect of surface tension and gravity reduced the local wall thickness by as much as 0.010 in. in one case. Some junctions had a small air bubble attached to them.

(iii) the wall thicknesses of the tubes were not uniform at any cross-section and varied somewhat in the axial direction. This variation was as much as 0.060 in. in one case.

These defects are illustrated in the selected photographs in Appendix A-1.

About three quarters of the thermocouples were defective (see Appendix A-2). The experiments were run, however, with these test sections and the defective junctions and wall thickness corrections were determined after the experiments. In this way, only the 'good' thermocouples together with their exact locations were used in analyzing the results according to the procedures outlined in Section 6.1.

Those thermocouples which were judged to be correct by visual observation were further tested for correctness of

operation by evaluating their extrapolated temperatures at different hot water temperatures. It can be shown by calculation using a standard heat transfer correlation for an annulus that, with the cold water flowrates used, the outside wall temperature of the test section should be essentially at the cold water temperature. Hence, a test for the correct operation of the thermocouple pair is to test whether the extrapolated outer wall temperature is close to the cooling water temperature. All thermocouple which were judged to be correct by visual observation met this test. The normalizing procedure as described in Section 6.1.2 to correct for varying wall thickness was also judged to be correct by this test.

Since in most cases, only one pair out of the five pairs of thermocouples installed was functioning properly, the temperature variation of the inside surface with length could not be studied. This, however, should not vary appreciably because of the heat transfer rates which existed.

It should also be mentioned that three thermocouple junctions at three different depths were imbedded in the 1¼ in. I.D. test sections at three different levels in the hope that it would provide test on the accuracy of the linear extrapolation. Unfortunately most of the junctions were defective.

CHAPTER 6

RESULTS

6.1 Treatment of experimental data

6.1.1 Flowrate at reversal

The flowrates indicated by the rotameter at reversal conditions were translated into mass flowrates by means of the calibration curves (Appendix E), which was then multiplied by the factor $\sqrt{(\rho_{T_f} / \rho_{T_{ref}})}$ to account for density variation with temperature. The upper and lower limits of flow reversal were established at ±0.013 lb/sec for the 3 and 4 in. test sections; ±0.008 lb/sec for the 2 in. test sections; and ±0.0025 lb/sec for the 1¼ in. test sections respectively. These limits also included the slight fluctuation of flow due to the instability of the system. Percentage error in flowrate calculations are shown in Appendix B-2.

6.1.2 Wall temperature estimation

The inside and outside wall temperatures were obtained by linear extrapolation of the two temperatures measured by thermocouples imbedded at two different depths. The pair of thermocouple being chosen for each test section is indicated in Appendix A-2.

An example of such an extrapolation is shown

in Figure 9. The depth of each thermocouple junction was normalized with respect to the local wall thickness to account for variation in wall thicknesses. All experimental runs using the same section but different hot fluid temperatures were plotted on the same graph. Theoretically they should all extrapolate to approximately the same cold wall temperature on the coolant side. The variation in the extrapolated cold wall temperature thus served to indicate the experimental error in the extrapolated hot wall temperatures as well. The hot wall temperatures were obtained by forcing the extrapolation lines to pass through the mean cold wall temperature. The error in wall temperature thus estimated varied from $\pm 0.5^{\circ}F$ to $\pm 2.0^{\circ}F$ as shown in Appendix B-2.

6.1.3 Physical properties

Physical properties such as density, viscosity, Prandtl number and $(g\beta/\upsilon^2)$ were obtained from Reference (23) and plotted as graphs as in Appendix D-2. The physical properties corresponding to experimental conditions were read off from these graphs at the film temperature T_f, which is defined as the mean of the inlet fluid bulk temperature T_b and extrapolated inside wall temperature T_w. The Grashof number was then calculated from

$$Gr = (g\beta/\upsilon^2)(D^3)(\Delta T) \qquad (6.1)$$

where $(\Delta T) = T_b - T_w$.

FIGURE 9 Determination of Wall Temperature by Normalised Linear Extrapolation of Experimental Measurements

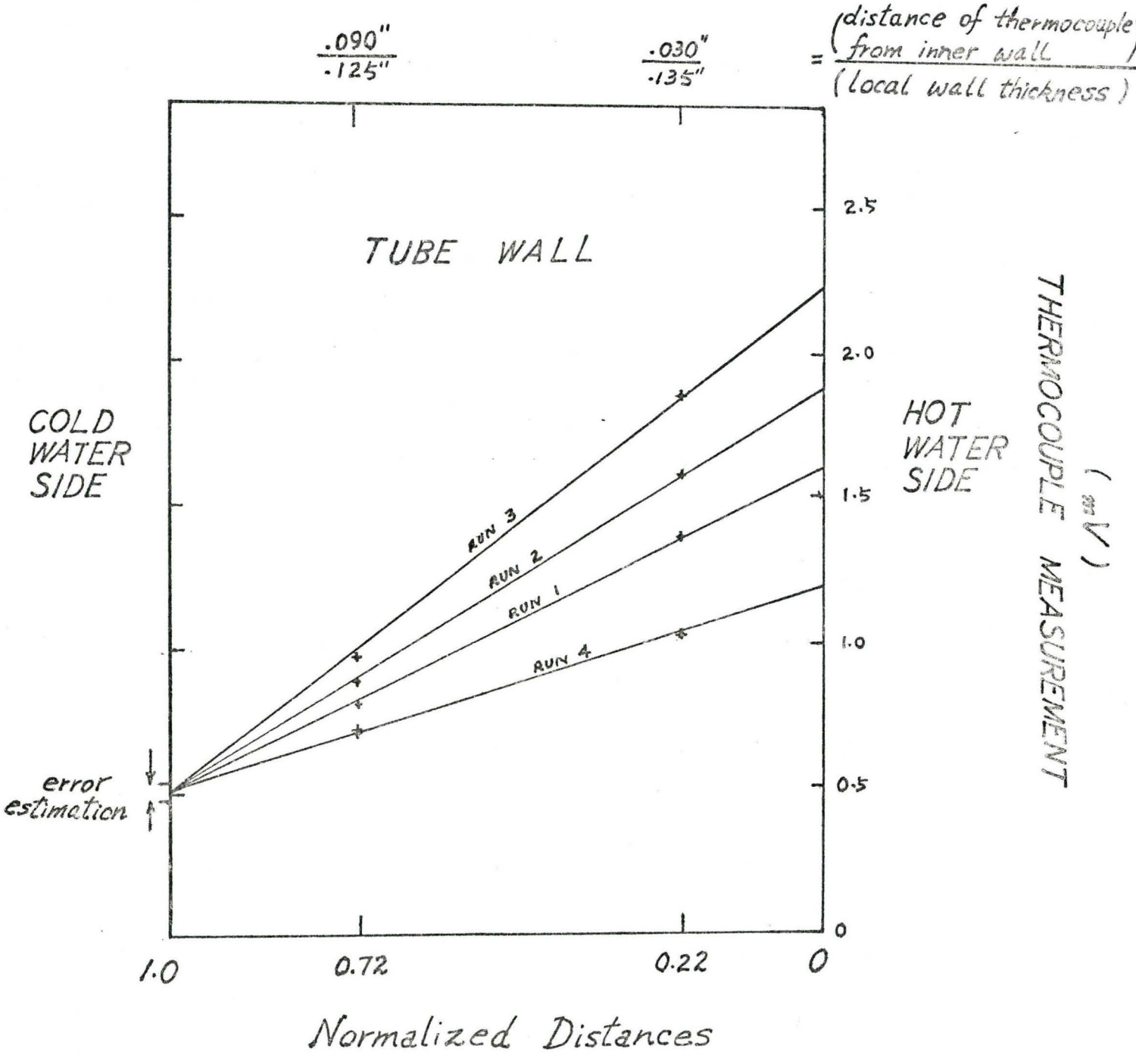

The percentage error in ΔT was then estimated for each run which vaired from ±2.4 to ±18.2% as shown in Appendix B-2. These calculated percentage errors in ΔT also represents the percentage error in the term $GrPr(\frac{d}{L})$ and will be shown as error bars on the Metais-Eckert plot.

6.2 Instability limits on the Metais-Eckert plot

The data obtained for the eight test sections are listed in Appendix B-1 as runs 1 to 38. These were translated into the dimensionless numbers Re and $GrPr(\frac{d}{L})$ at the point of instability and plotted on the Metais-Eckert plot in Figure 10. The error bars indicate the estimated experimental error in temperature determination and the limits of reversal for each run.

The data when plotted, showed that the reversal lines for tubes of the same diameter but different lengths appeared to be parallel to each other but laterally displaced.

The results for the 1¼ in. I.D. sections showed a different behaviour from the others in that the temperatures of the inside wall were much lower. Furthermore the dye was observed to descend as a continuous streak, that is it did not disperse into multiple wavy streaks as was observed with the larger diameter test sections. Both of these observations suggest that the flow was essentially laminar (as is suggested by the low Reynolds numbers for this test section). As further evidence of a different flow regime, it is noted that the buoyancy

Figure 10

Plotting of Experimental and Theoretical Results on the Metais-Eckert Plot

Key to Symbols:

(1) Experimental Results

□	3	in.	I.D.	x 3	ft.	Section.
■	3	"		x 2	"	.
△	2	"		x 3	"	.
▲	2	"		x 2	"	.
○	4	"		x 3	"	.
●	4	"		x 2	"	.
▽	$1\frac{1}{4}$	"		x 2	"	.
▼	$1\frac{1}{4}$	"		x 1	"	.

(2) Theoretical Results

X	4	in.	I.D.	x 3	ft.	Section.
⊥	4	"		x 2	"	.
T	3	"		x 3	"	.

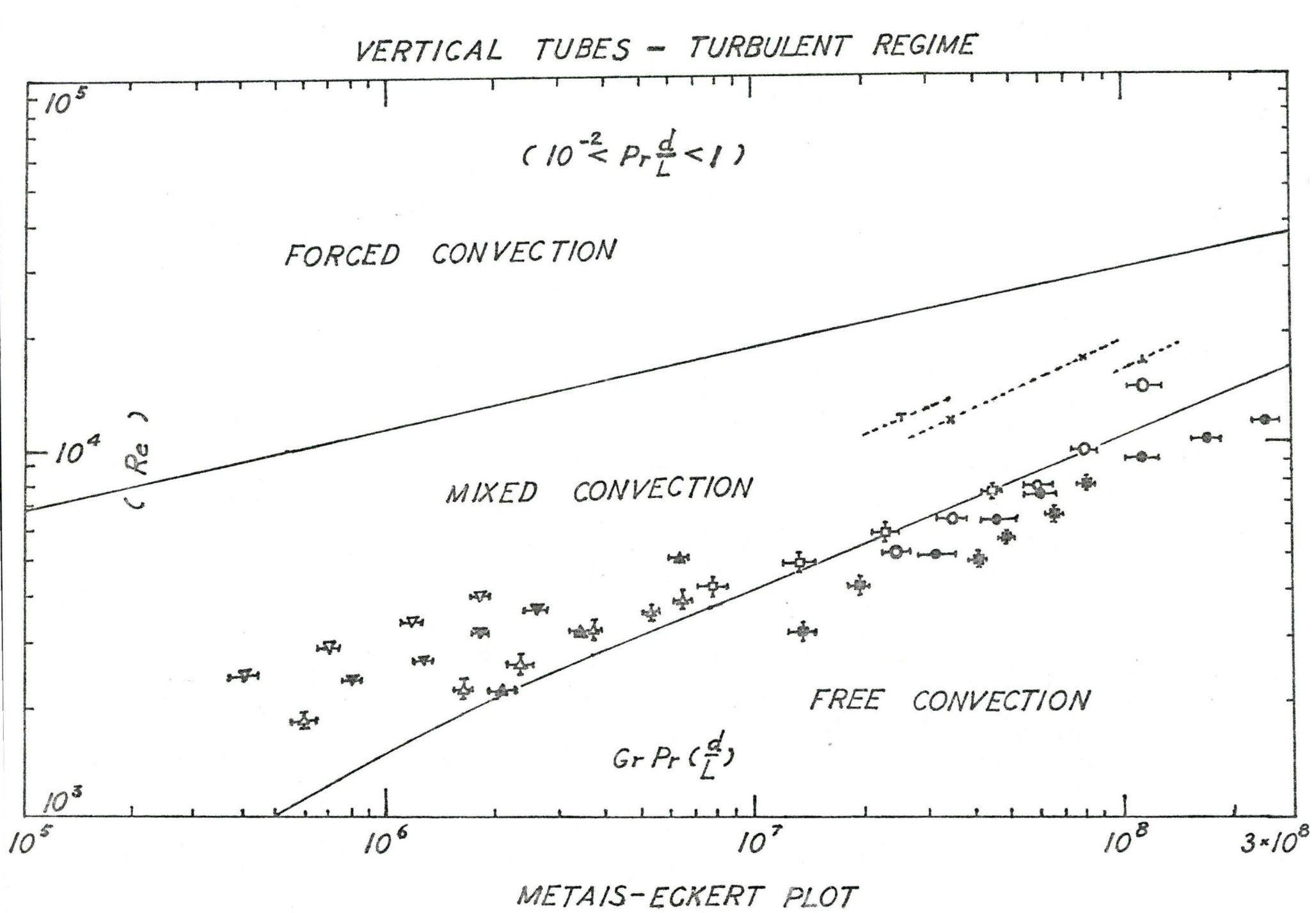
VERTICAL TUBES – TURBULENT REGIME
10^5
$(10^{-2} \leq Pr\frac{d}{L} < 1)$
FORCED CONVECTION
10^4
(Re)
MIXED CONVECTION
FREE CONVECTION
$Gr\,Pr\,(\frac{d}{L})$
10^3
10^5
10^6
10^7
10^8
3×10^8
METAIS-ECKERT PLOT

to inertial forces (as indicated by the ratio Gr/Re^2 in Appendix B-3) was much less for the 1¼ in. tube than for the larger diameters. In most cases (Runs 1 to 30) for these larger diameter tubes, this ratio was greater than unity; this ratio, however, is less than unity for the eight cases for the 1¼ in. diameter tubes (Runs 31 to 38). Because these small diameter runs were suspected as being in another flow regime (laminar-turbulent mixed transition regime), the results from them are not treated together with the other results in the following analysis.

6.3 Regression of experimental data

Since the Metais-Eckert plot did not correlate the instability data but showed separate lines for different systems, further analysis is necessary. In an attempt to ascertain the importance of various experimental variables or dimensionless groups, a linear multiple regression analysis was carried out using the data for the 2, 3 and 4 in. diameter tubes.

The data were first regressed in a three parameter model:

$$\ell n(Re) = a' + b'\{\ell n(\frac{d}{L}) - \overline{\ell n(\frac{d}{L})}\} + c'\{\ell n(GrPr) - \overline{\ell n(GrPr)}\} \qquad (6.2)$$

which resulted in the following correlation:

$$Re = 7.78\ (\frac{d}{L})^{0.145}(GrPr)^{0.356} \qquad (6.3)$$

Because the results indicate a small $(\frac{d}{L})$ effect, the same data were regressed according to the model:

$$\ell n(Re) = a + b\ \{\ell n(GrPr) - \overline{\ell n(GrPr)}\} \qquad (6.4)$$

with the result:

$$Re = 3.12\ (GrPr)^{0.387} \quad . \qquad (6.5)$$

A test for the extra sum of squares was performed on the two models (Equations (6.3) and (6.5)) based on their residual sum of squares, and it was shown that the addition of the $(\frac{d}{L})$ term in the three-parameter model was not significant at the 95% confidence level (Appendix C-3).

The data relative to the two-parameter model are shown on Figure 11. Details of regression can be found in Appendices C-1 and C-2.

Figure 11

Experimental and Theoretical Results
As shown on the Regressed Plot

Key to Symbols:

(1) Experimental Results

□	3	in.	I.D. x 3	ft.	Section.
■	3	"	x 2	"	.
△	2	"	x 3	"	.
▲	2	"	x 2	"	.
○	4	"	x 3	"	.
●	4	"	x 2	"	.

(2) Theoretical Results

X	4	in.	I.D. x 3	ft.	Section.
⊥	4	"	x 2	"	.
T	3	"	x 3	"	.

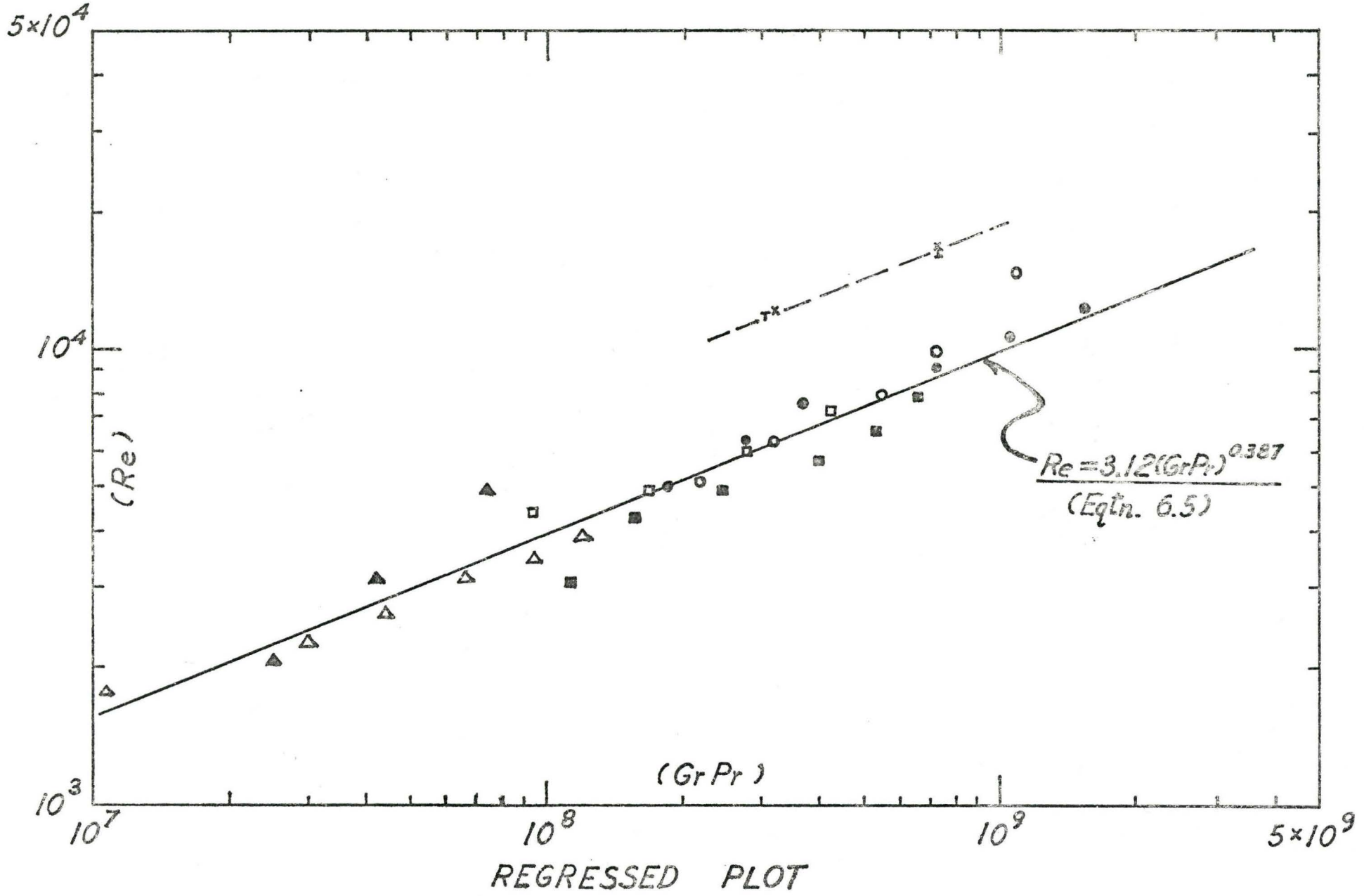

REGRESSED PLOT

CHAPTER 7
DISCUSSION

The applicability of the Metais-Eckert plot to correlating the flow reversal results was investigated via the following two hypotheses:

(i) that reversal conditions can be represented by a single line in the mixed convection region. This also implies that as L is increased, while the buoyancy force is maintained constant, the flowrate at reversal would decrease, and

(ii) that reversal conditions are represented by a series of parallel lines in the mixed convection region, with the reversal line for a shorter section lying below that for a longer one. This implies that given the same buoyancy forces, the flowrate at reversal would decrease with the length of the test section.

Result obtained by plotting both experimental and theoretical data were in support of the second hypothesis (see Figure 10 on page 46). This implies that the Metais-Eckert plot is inadequate for accurate flow reversal predictions. In fact, the diameter and length effects were improperly accounted for by the $(\frac{d}{L})$ parameter on the plot.

The significance of the $(\frac{d}{L})$ effect was then examined by regression analysis of the experimental data. As indicated this regression analysis shows that under the present experimental conditions, the data obtained are better correlated without the $(\frac{d}{L})$ factor. The data fell on a near straight

line on the Re versus GrPr plot (Figure 11 on Page 49). However, the validity of such a plot is limited to relatively short heat transfer sections of $6 \leq (\frac{L}{d}) \leq 18$ only. For longer heat transfer sections, the diameter and length factors may be significant, in which case the parameter $(\frac{L}{d})$ will have to be included.

Also, the resulting regression of:

$$Re = k\ (GrPr)^{0.387} \tag{7.1}$$

can be expressed in the following form:

$$\frac{Gr}{Re^{2.58}} = \frac{k'}{Pr} = F(\text{Physical properties of fluid}) \tag{7.2}$$

Equation (7.2) suggests that the ratio of buoyancy forces to a combination of viscous and inertial forces is the determining factor in the slowing down of turbulently flowing fluid. The importance of the viscous force in such a system is probably brought about by the relaminarization of the fluid at the wall under high opposing buoyancy forces.

Although both the experimental and theoretical results were successfully correlated as straight lines on the regressed plot, the theoretical flowrates at reversal are consistently higher than the experimental ones. The discrepancy, however, can be reduced by an appropriate increase in the momentum eddy diffusivity in the theoretical analysis which will result in a reduction of flow velocity at reversal for a given buoyancy force. This increase in the momentum eddy diffusivity is consistent with Khosla's[3] observation that the effective eddy conductivity increases with the ratio

of Gr/Re^2 of the system. The constitutive relationships for eddy diffusivities fail to take the buoyancy effect into account.

The length effect was further investigated in a tentative (least square) plot of Gr/Re^2 against Re at reversing conditions (Figure 12). This, when compared to the Gr/Re against Re plot of Gensini (Figure 2 on Page 12) for the transition to asymmetric flow in laminar flow, appeared to be a mirror image of the other. A possible explanation for this is that the heat transfer rate in turbulent opposing flows increases with the Reynolds number at a much faster rate than in laminar opposing flows. The length effects are similar in both cases as expected, where a longer length would require a smaller heat flux than a shorter one to reach the same state of instability or reversal. In addition, the data for turbulent flow showed a larger scattering because of the increased instability in the system.

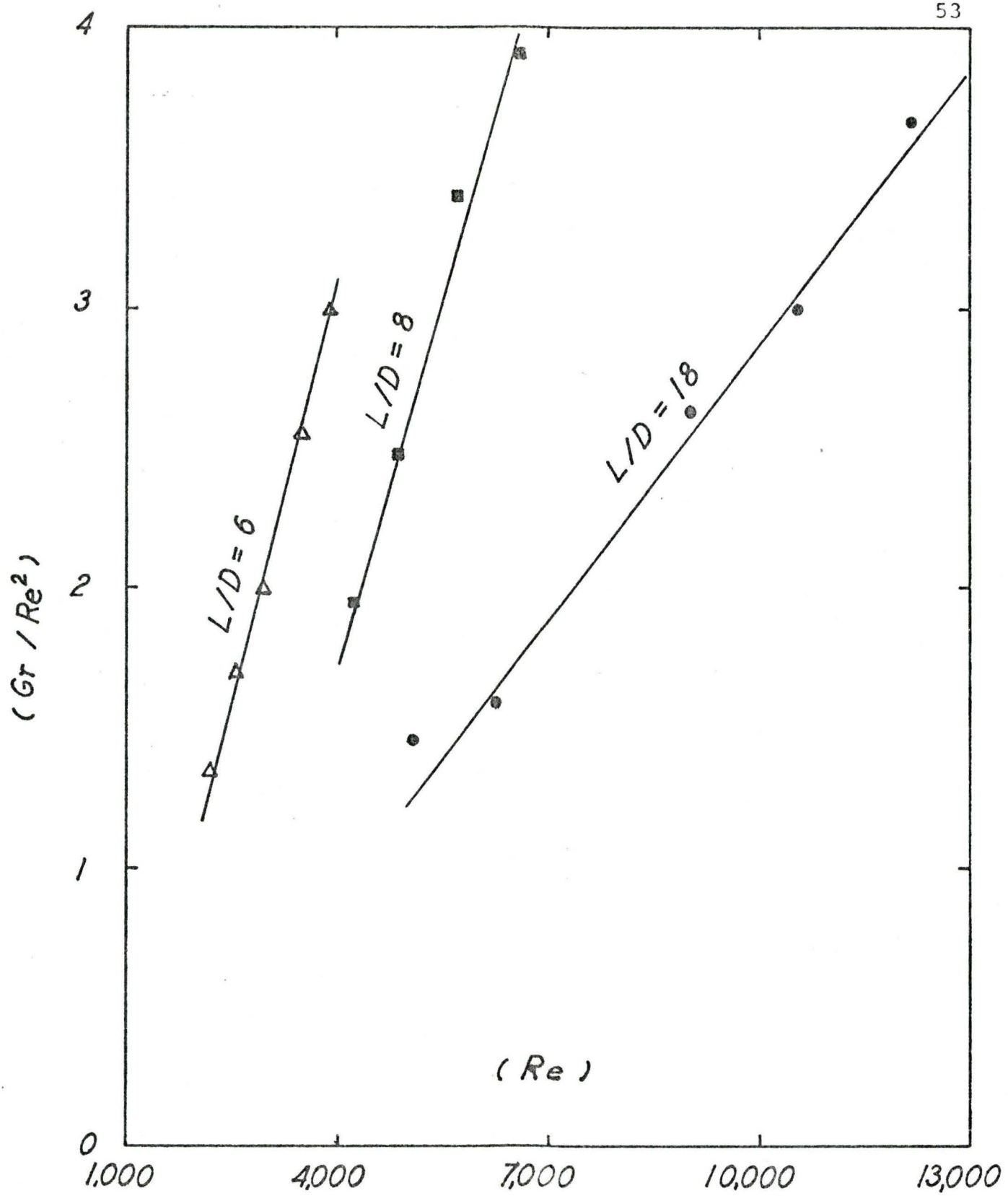

Figure 12 Flow Conditions at Reversal Showing Length and Buoyancy Effects

CHAPTER 8

CONCLUSIONS

1. Flow reversal conditions in the turbulent opposing convection regime was investigated by the cooling of upflow water and the data were correlated in the form:

$$Re = 3.12\ (GrPr)^{0.387}$$

which is valid for $6 \leq (L/d) \leq 18$.

2. The reversal conditions can be expressed in a more meaningful form:

$$\frac{Gr}{Re^{2.58}} \approx \text{constant}$$

where the constant is a function of the average Prandtl number of the fluid.

3. The Metais-Eckert plot is not suitable for flow reversal correlation because of the improper inclusion of the parameter $(\frac{d}{L})$.

4. The data obtained in the present experiment indicates that the turbulent mixed convection region for opposing systems seems to lie at positions lower than those indicated in the Metais-Eckert plot.

CHAPTER 9

RECOMMENDATIONS FOR FUTURE WORK

1. Heat transfer sections with larger $(\frac{L}{d})$ ratio could be used to further investigate the effect of the length of heat transfer section on flow reversal.

2. With existing equipment, one could try to observe flow reversal in aiding flow situations by placing the cathode at the centre-line at the exit end of the tube for dye emission.

3. The apparatus can be improved by incorporating the following modifications:

   (a) The performance of the thermocouple junctions can be improved by noting the following:

      (i) the tip of the slot where the hot junction is inserted onto the heat transfer surface could be enlarged so as to reduce the chance of having air trapped in it,

      (ii) actually some of the air bubbles were present before filling the slots; these came from mixing the acrylic cement with its hardener by stirring. Unless a different cement with similar thermal properties is used, this effect may be unavoidable. In any event, care should be exercised in the mixing process to try to avoid incorporating air bubbles.

(b) Additional thermocouples should be placed at locations to measure:

(i) the temperature of hot fluid coming out of the heat transfer section after being cooled,

(ii) the inlet cold water temperature,

(iii) the outlet cold water temperature.

These additional measurements will provide data for the calculation of heat transfer coefficients and for checking the wall temperatures determined from extrapolation.

(c) The storage tanks for the solution should be placed on the second floor level, so that the system can be emptied by pumping the fluid through a side-arm into the storage tanks. Loading the system would simply be by gravity from the storage tanks to the heating tank on the first floor. This requires the installation of a two-way valve on the upcoming pipe from the pump at the second floor level.

(d) Better control of the hot water flowrate near flow reversal conditions can be achieved by by-passing small fractions of the fluid (through a small copper pipe) around the test section to the receiving tank A. A small rotameter will be required to register the amount of bypass.

(e) At present the temperature of the hot fluid is restricted to below 175^{o}F for the 3 and 4 in. tubes; distortion was observed to occur for the 2 in. tube at approximately 160^{o}F and for the 1¼ in. tube at 150^{o}F.

These limitations might be overcome by the use of copper sections and short transparent sections just below the insulated electrodes. However one will have to worry about thermal expansion, leaking problems, matching diameters to avoid flow disturbance and lighting for visualization in this case. It may however allow better control of wall thickness.

REFERENCES

(1) SCHEELE,G.F. & HANRATTY,T.J., J. Fluid Mech., 14, 244(1962).

(2) HERBERT,L.S. & STERNS,U.J., Private Communication, CSIRO,Australia(1971).

(3) KHOSLA,J., Ph.D. Thesis, Chemical Engineering, McMaster University(1973).

(4) ECKERT,E.R.G. & DIAGUILA,A.J., Trans. ASME, 76, 497 (1954).

(5) THOMAS,J.C., Ph.D. Thesis, Chemical Engineering, University of Akron(1971).

(6) GENSINI,F.D., Ph.D. Thesis, Chemical Engineering, Cornell University(1972).

(7) PINKEL,B., Trans. ASME, 76, 305(1954).

(8) DEISSLER,R.G., Trans. ASME, 76, 73(1954).

(9) HALL,W.B. & JACKSON,J.D., ASME-AIChE Heat Transfer Conference, Minneapolis, P69-HT-55(1969).

(10) VAN DRIEST,E.R., J. Aeronautical Soc., 1007(1956).

(11) SPALDING,D.B., J. App. Mech., 28, 455(1961).

(12) BOURNE,D.E., J. Aerospace Sci., 26, 459(1959).

(13) QUARMBY,A. & QUIRK,R., Int. J. Heat & Mass Transfer, 15, 2309(1972).

(14) METAIS,B. & ECKERT,E.R.G., J. Heat Transfer, 86, 295(1964).

(15) SCHEELE,G.F., ROSEN,E.M. & HANRATTY,T.J., Can. J. Chem. Eng., 38, 67(1960).

(16) ROSEN,E.M., Ph.D. Thesis, University of Illinois(1959).

(17) BROWN,C.K. & GAUVIN,W.H., Can. J. Chem. Eng., 43, 317(1965).

(18) HALL,W.B. & PRICE,P.H., Instn. Mech. Engrs. Sym., P-C113(1971).

(19) HANRATTY,T.J., ROSEN,E.M. & KABEL,R.L., Ind. Eng. Chem., 50, 815(1958).

(20) SHERWOOD,T.K., SMITH,K.A. & FOWLES,P.E., Chem. Eng. Sci., 23, 1225(1968).

(21) POPOVICH,A.T. & HUMMEL,R.L., Chem. Eng. Sci., 22, 21(1967).

(22) BAKER,J., J. Fluid Mech., 26, part 3, 573(1966).

(23) KREITH,F., "Principles of Heat Transfer", International Textbook Co., 2nd Edition, Scranton, Penn.(1965).

(24) "INDICATORS", Edited by Edmund Bishop, Pergamon Press, 1st edition(1972).

NOMENCLATURE

a, R_o	Radius of pipe, ft.
C_p	Heat capacity, BTU/lb-^oF.
D	Diameter of pipe, ft.
g_c	Gravitational constant, lb_m-ft/lb_f-sec^2.
h	Heat transfer coefficient, BTU/ft^2-hr-^oF.
k	Thermal conductivity, BTU/ft-hr-^oF.
L	Length of heat transfer section, ft.
q'	Calculated heat flux at the tube wall, BTU/hr-ft^2.
r	Radial location, ft.
T	Temperature, ^oF or ^oR as indicated.
u	Axial velocity, ft/sec.
v	Radial velocity, ft/sec.
x	Axial distance from the entrance, ft.
y	Distance from wall, (R_o-r), ft.

Dimensionless Groups

Gr, $(N_{Gr})_D$	Grashof number, $D^3 g\beta(T_w-T_o)/\nu^2$.
Gr_t	Grashof number based on the difference between the entrance temperature and the jacket temperature, $a^3 g\beta(T_j-T_o)/\nu^2$.
Gz	Graetz number, $Re_a Pr\ a/x$.
Nu, N_{Nu}	Nusselt number, hD/k.
Pr	Prandtl number, $C_p\mu/k$.
Pr_t	Turbulent Prandtl number, ϵ/ϵ_h.
Re, $2Re_a$, $2N_{Re_a}$	Reynolds number, DG/μ.
$N_{Grq'}$	Grashof number based on measured heat flux, $a^4 g\beta q'/k\nu^2$.

Greek Letters

ϵ	Eddy kinematic viscosity, ft^2/sec.
ϵ_h	Eddy thermal diffusivity, ft^2/sec.
ℓ	Mixing length, ft.
μ	Dynamic viscosity, lb/ft-sec.
ν	Kinematic viscosity, μ/ρ, ft^2/sec.
ρ	Density, lb/ft^3.
τ	Shear stress, lb_f/ft^2.

Subscripts

o = inlet j=jacket b=bulk f=film w=wall t=turbulent

APPENDIX A-1: VISUAL OBSERVATION OF THERMOCOUPLE JUNCTIONS IMBEDDED IN TUBE WALL SHOWING THEIR DEFECTS

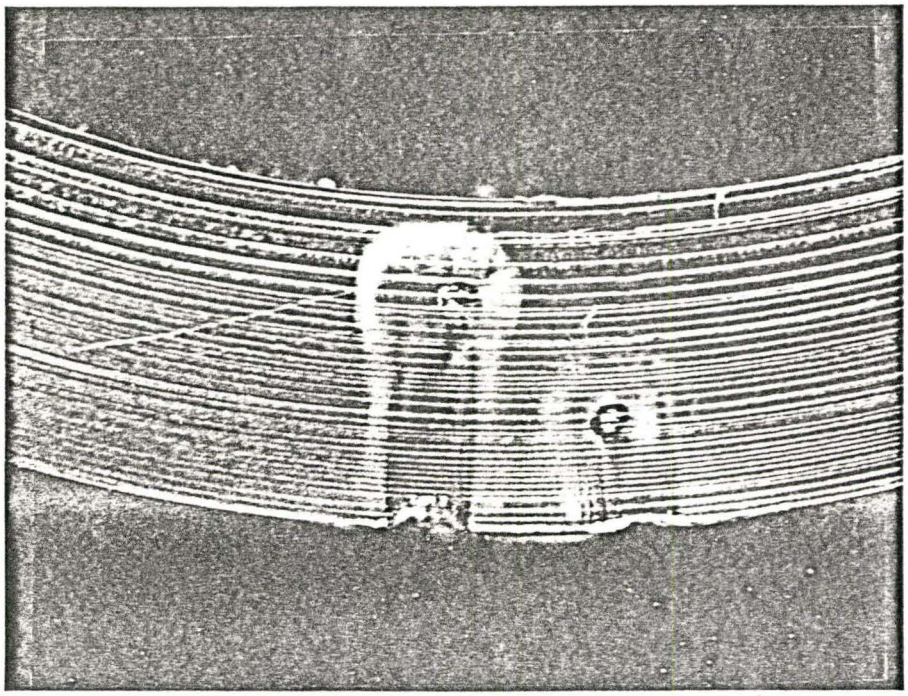

Figure A-1 Thermocouple Junction with No Defect from 1-1/4"x1' Section (Pair No. 1)

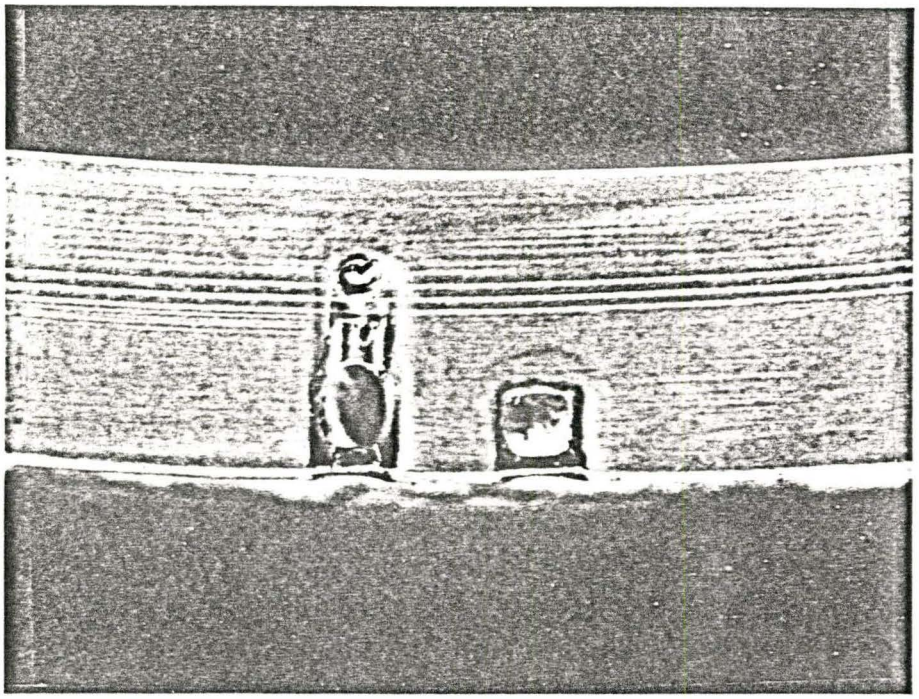

Left: Junction covered but incomplete fill up of slot.

Right: Junction not covered, slot covered but unfilled.

Figure A-2 Thermocouple Junction with Defects from 4"x2' Section (Pair No.5)

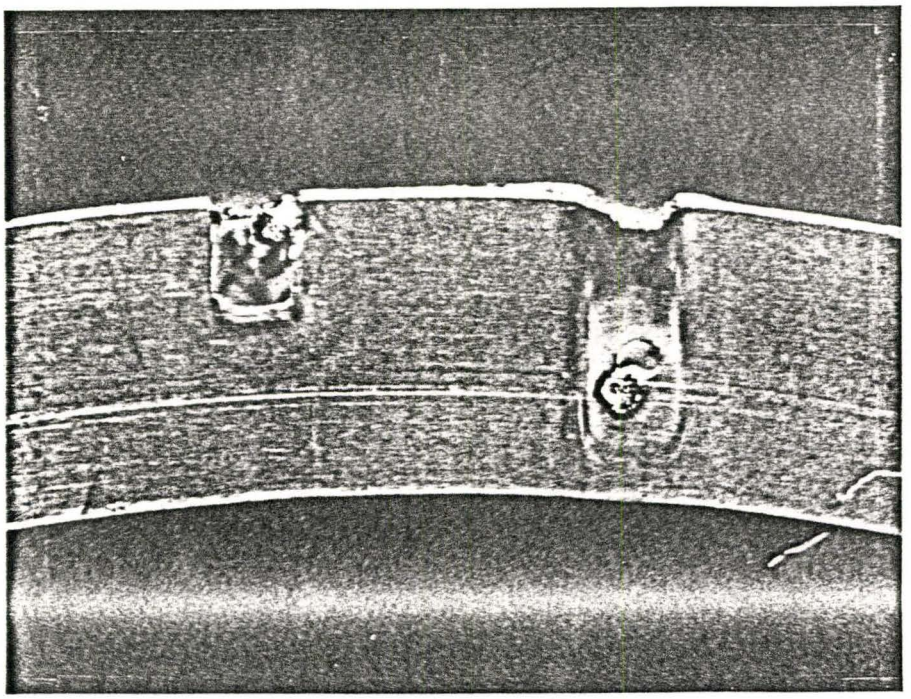

Left: Junction "floated" to the surface.

Right: Air bubble attached to hot junction.

Figure A-3 Thermocouple Junction with Defects from 2"x2' Section (Pair No.1)

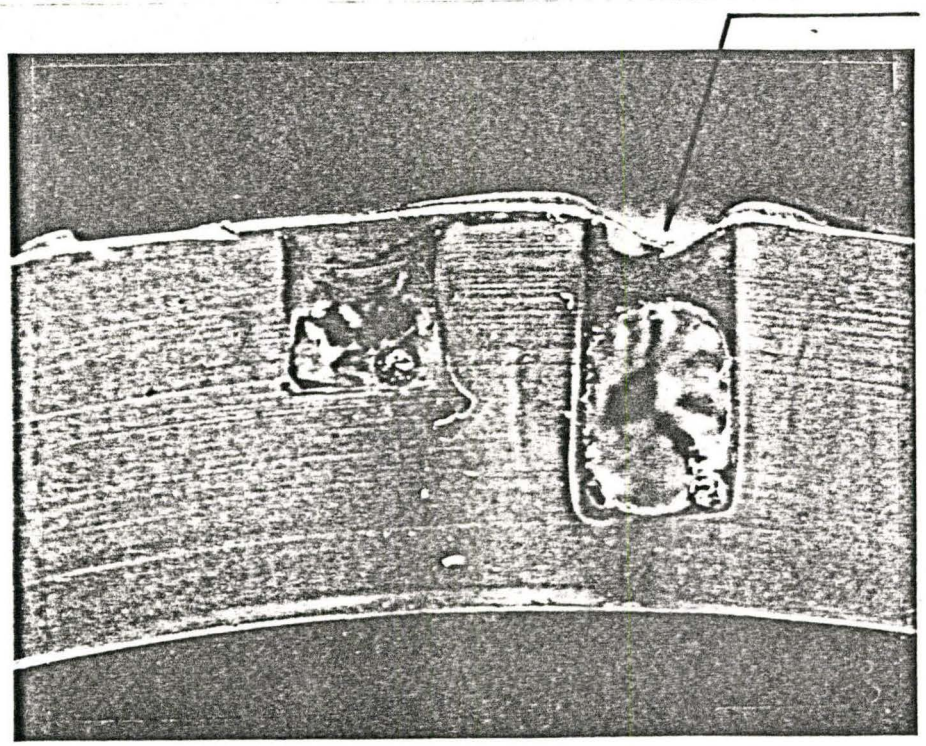

"Dip" on surface of slot.

Left: Both interior and junction unfilled.

Right: Large unfilled interior and partially covered junction.

Figure A-4 Thermocouple Junction with Defects from 2"x3' Section (Pair No.3)

APPENDIX A-2 Wall Thicknesses, Locations and Conditions of Thermocouples

TABLE A-1 CONDITIONS OF THERMOCOUPLES

Test Section	No.	Distance From Exit End(in)	Distance From Inside Surface(in)	Local Wall Thickness	Defects
1¼" x 1'	1*	1.0	.090	.140	-
			.035	.130	-
	2	3.5	.093	.150	-
			.060	.152	Bubble at stem
			-	-	Large hole
	3	6.5	.095	.145	-
			.060	.145	-
			-	-	Large hole
	4	9.5	.094	.135	-
			.065	.145	-
			-	-	Large hole
	5	11.0	-	-	Large hole
			-	-	Large hole
1¼" x 2'	1	1.0	.120	.160	-
			-	-	Large hole
	2	3.5	.105	.150	-
			.080	.140	Bubble at Junction
			-	-	Large hole
	3*	6.5	.108	.150	-
			.057	.145	-
			-	-	Large hole
	4	9.5	.095	.180	-
			.075	.180	-
			-	-	Large hole

....Cont'd

TABLE A-1 Cont'd

Test ection	No.	Distance From Exit End(in)	Distance From Inside Surface(in)	Local Wall Thickness (in.)	Defects
	5	11.0	.110	.185	-
			-	-	Large hole
2"x 2'	1	1.0	.110	.120	Large hole
			.035	.120	Bubble at Wire
	2	4.0	-	-	Float to Surface
			.040	.110	-
	3*	8.0	.095	.135	-
			.035	.145	-
	4	12.0	-	-	Bubble
			-	-	Bubble
	5	18.0	.085	.125	-
			-	-	Not filled
2"x 3'	1	1.0	.085	.150	-
			.055	.155	Bubble at stem
	2	6.0	.090	.150	-
			.070	.155	Bubble at stem
	3	12.0	-	-	Small hole
			-	-	Large hole
	4*	18.0	.095	.160	-
			.040	.165	-
	5	27.0	-	-	Large hole
			-	-	Large hole
3"x 2'	1*	1.0	.085	.130	-
			.045	.130	-
	2	4.0	.101	.135	-
			.050	.135	Large hole
	3	8.0	.090	.120	-
			.040	.125	Not filled
	4	12.0	.090	.125	Bubble
			.090	.120	Floated up

.....Cont'd

TABLE A-1 Cont'd

Test Section	No.	Distance From Exit End (in)	Distance From Inside Surface (in)	Local Wall Thickness (in.)	Defects
	5	18.0	.100	.125	-
			.040	.135	Not filled
3" x 3'	1	1.5	.105	.130	-
			-	-	Large hole
	2	7.5	.070	.135	Bubble at stem
			.022	.135	-
	3	13.5	.048	.135	Bubble at Junction
			.020	.130	-
	4*	19.5	.090	.125	-
			.030	.130	-
	5*	25.5	.090	.125	-
			.030	.135	-
	6*	31.5	.090	.130	-
			.022	.132	-
	7	35.5	.100	.120	-
			-	-	Large hole
4" x 2'	1	1.0	.080	.130	-
			.065	.075	Not filled
	2*	4.0	.120	.150	-
			.070	.135	Bubble at stem
	3	8.0	.120	.140	-
			-	-	Not filled
	4	12.0	.060	.120	-
			-	-	Large bubble
	5	18.0	-	-	Large hole
			-	-	Large hole
4" x 3'	1	1.0	.090	.130	-
			-	-	Hole near wire
	2	6.0	.050	.092	-
			-	-	Floated to top

.....Cont'd

TABLE A-1 Cont'd

Test Section	No.	Distance From Exit End(in)	Distance From Inside Surface(in)	(in.) Local Wall Thickness	Defects
	3*	12.0	.080	.120	-
			.025	.125	-
	4	18.0	-	-	Large hole
			-	-	Large hole
	5	27.0	-	-	Large hole

* The thermocouples marked with asterisks were used for wall temperature extrapolation.

APPENDIX B EXPERIMENTAL DATA

APPENDIX B-1 Experimental Results at Flow Reversal

TABLE A-2

Run	Test Section	(^{o}F) Fluid Temp	Average Flow at Reversal (lb/sec)	Extrapolated Wall Temp (^{o}F)
1	3" x 3'	120	.3880	104
2	"	137	.4180	117
3	"	156	.4480	132
4	"	99	.4193	86
5	3" x 2'	96	.3195	78
6	"	120	.4036	95
7	"	152	.4269	118
8	"	110	.3739	92
9	"	138	.4128	107
10	"	164	.4710	126
11	2" x 3'	88	.1258	82
12	"	109	.1296	98
13	"	123	.1344	110
14	"	136	.1441	120
15	"	149	.1463	130
16	"	163	.1461	142
17	2" x 2'	98	.1372	86
18	"	123	.1593	111
19	"	147	.2084	132
20	4" x 3'	97	.6987	83
21	"	124	.8165	103
22	"	108	.7530	92
23	"	138	.9195	116
24	"	153	1.2404	125
25	4" x 2'	98	.660	87
26	"	109	.735	96
27	"	121	.805	107
28	"	139	.845	116
29	"	151	.910	124
30	"	166	.950	133
31	1¼" x 2'	97	.097	76
32	"	112	.104	83
33	"	129	.109	90
34	"	144	.114	97
35	1¼" x 1'	93	.101	69
36	"	105	.108	75
37	"	116	.114	80
38	"	130	.122	87

APPENDIX B-2 Flow Reversal Results in Dimensionless Forms

TABLE A-3

RUN	Re	Gr	Pr	d/L	GrPr(d/L)	Gr/Re^2
1	4885	4.25×10^{7}	3.95	0.0833	1.40×10^{7}	1.78
2	5990	8.19×10^{8}	3.40	"	2.32×10^{7}	2.28
3	7432	1.47×10^{7}	2.90	"	3.56×10^{7}	2.67
4	4356	1.88×10^{7}	4.95	"	7.75×10^{6}	0.99
5	3099	2.11×10^{7}	5.35	0.1250	1.41×10^{7}	2.20
6	4894	5.86×10^{8}	4.15	"	3.04×10^{7}	2.45
7	6589	1.70×10^{8}	3.15	"	6.69×10^{7}	3.92
8	4232	3.49×10^{7}	4.45	"	1.94×10^{7}	1.95
9	5721	1.11×10^{8}	3.55	"	4.94×10^{7}	3.40
10	7865	2.38×10^{8}	2.75	"	8.16×10^{7}	3.80
11	1780	1.94×10^{6}	5.50	0.0555	5.94×10^{5}	0.61
12	2250	6.75×10^{6}	4.35	"	1.63×10^{6}	1.33
13	2632	1.17×10^{7}	3.75	"	3.65×10^{6}	1.69
14	3146	1.96×10^{7}	3.35	"	3.65×10^{6}	1.98
15	3494	3.12×10^{7}	3.00	"	5.20×10^{6}	2.56
16	3916	4.57×10^{7}	2.66	"	6.75×10^{6}	2.98
17	2109	5.00×10^{6}	5.00	0.0833	2.08×10^{6}	1.12
18	3160	1.11×10^{7}	3.75	"	3.47×10^{6}	1.11
19	4975	2.47×10^{7}	3.00	"	6.16×10^{6}	0.99
20	5134	4.25×10^{7}	5.15	0.1111	2.43×10^{7}	1.61
21	7797	1.40×10^{8}	3.90	"	6.07×10^{7}	2.30
22	6253	6.96×10^{7}	4.53	"	3.50×10^{7}	1.78
23	9894	2.12×10^{8}	3.40	"	8.00×10^{7}	2.16
24	14807	3.56×10^{8}	3.05	"	1.21×10^{8}	1.63
25	5083	3.77×10^{7}	4.98	0.1667	3.13×10^{7}	1.46
26	6290	6.26×10^{7}	4.40	"	4.59×10^{7}	1.58
27	7654	9.46×10^{7}	3.85	"	6.07×10^{7}	1.61
28	9037	2.17×10^{8}	3.40	"	1.23×10^{8}	2.65
29	10616	3.40×10^{8}	3.08	"	1.74×10^{8}	3.02
30	12189	5.43×10^{8}	2.80	"	2.53×10^{8}	3.65
31	2351	1.53×10^{6}	5.40	0.0495	4.08×10^{5}	0.28
32	2840	3.00×10^{6}	4.70	"	6.98×10^{5}	0.37
33	3367	5.97×10^{7}	4.08	"	1.21×10^{6}	0.53
34	3892	1.00×10^{7}	3.60	"	1.78×10^{6}	0.66
35	2293	1.40×10^{6}	5.80	0.0990	8.04×10^{5}	0.27
36	2720	2.47×10^{6}	5.15	"	1.26×10^{6}	0.34
37	3146	3.84×10^{6}	4.65	"	1.76×10^{6}	0.39
38	3724	6.53×10^{6}	4.10	"	2.65×10^{6}	0.47

APPENDIX B-3 Error Analysis on Temperature Estimation

From Section 6.1.3, $\Delta T = T_b - T_w$,

therefore percentage error on $\Delta T = \frac{\delta(\Delta T)}{\Delta T} \times 100\%$

$$\simeq \frac{\delta(T_w)}{\Delta T} \times 100\% .$$

TABLE A-4

RUN	ΔT ($^{\circ}$F)	δT_w ($^{\circ}$F)	± % Error on ΔT
1	16	± 1.5	9.4
2	20	"	7.4
3	24	"	6.2
4	13	"	11.8
5	18	± 1.5	8.3
6	25	"	6.0
7	34	"	4.4
8	18	"	8.3
9	31	"	4.8
10	38	"	3.9
11	6	± 0.5	8.3
12	11	"	4.5
13	13	"	3.8
14	16	"	3.1
15	19	"	2.6
16	21	"	2.4
17	12	± 1.0	8.3
18	12	"	8.3
19	15	"	6.7
20	14	± 2.0	14.8
21	21	"	9.5
22	16	"	12.5
23	22	"	9.1
24	28	"	7.3
25	11	± 2.0	18.2
26	13	"	15.4
27	14	"	14.3
28	23	"	8.9
29	27	"	7.4
30	33	"	6.2
31	21	± 1.5	7.1
32	30	"	5.1
33	39	"	3.9
34	47	"	3.2
35	24	± 1.5	6.3
36	30	"	5.0
37	36	"	4.2
38	44	"	3.4

TABLE A-5

APPENDIX B-4 Upper and Lower Limits on Reversal Flowrates

Run	Flowrate At Reversal (lb/sec)	Experimental Limits (lb/sec)	Percentage Limits	Upper and Lower Limits on Re
1	.388	± 0.013	± 3.4	± 166
2	.418	± "	± 3.1	± 186
3	.448	± "	± 2.9	± 216
4	.419	± "	± 3.1	± 135
5	.320	± 0.013	± 3.2	± 99
6	.404	± "	± 3.2	± 157
7	.427	± "	± 3.0	± 198
8	.374	± "	± 3.5	± 148
9	.413	± "	± 3.1	± 177
10	.471	± "	± 2.8	± 220
11	.126	± 0.008	± 6.3	± 112
12	.130	± "	± 6.2	± 140
13	.134	± "	± 6.0	± 158
14	.144	± "	± 5.6	± 176
15	.146	± "	± 5.5	± 192
16	.146	± "	± 5.5	± 215
17	.137	± 0.008	± 5.8	± 122
18	.159	± "	± 5.0	± 158
19	.208	± "	± 3.8	± 189
20	.699	± 0.013	± 1.8	± 92
21	.817	± "	± 1.6	± 125
22	.753	± "	± 1.7	± 106
23	.920	± "	± 1.4	± 139
24	1.240	± "	± 1.0	± 148
25	.659	± 0.013	± 2.0	± 102
26	.733	± "	± 1.8	± 113
27	.802	± "	± 1.6	± 122
28	.840	± "	± 1.5	± 136
29	.903	± "	± 1.4	± 149
30	.941	± "	± 1.4	± 171
31	.097	± 0.0025	± 2.6	± 61
32	.104	± "	± 2.4	± 68
33	.109	± "	± 2.3	± 77
34	.114	± "	± 2.2	± 86
35	.101	± 0.0025	± 2.5	± 57
36	.108	± "	± 2.3	± 63
37	.114	± "	± 2.2	± 69
38	.122	± "	± 2.0	± 74

APPENDIX C REGRESSION OF EXPERIMENTAL DATA

APPENDIX C-1 Regression of data using a three parameter model

The experimental data obtained from runs 1 to 30 were regressed according to the model

$$\ell n(Re) = a' + b'\{\ell n(\frac{d}{L}) - \overline{\ell n(\frac{d}{L})}\} + c'\{\ell n(GrPr) - \overline{\ell n(GrPr)}\} \quad (A\text{-}1)$$

using a linear least square regression program.

From experimental data, $\ell n(\frac{d}{L}) = -2.298$

and $\overline{\ell n(GrPr)} = 19.176$.

Results obtained with regression showed that

$a' = 8.555$, $b' = 0.145$ and $c' = 0.356$.

Now Equation (A-1) can also be written in the following form as:

$$\ell n(Re) - \ell n(d') = b'\ \ell n(\frac{d}{L}) + c'\ell n(GrPr) \quad (A\text{-}2)$$

where

$$\ell n(d') = a' - b'\overline{\ell n(\frac{d}{L})} - c'\overline{\ell n(GrPr)} \quad (A\text{-}3)$$

or

$$Re = d'(\frac{d}{L})^{b'}(GrPr)^{c'} \quad (A\text{-}4)$$

With the above values for a',b' and c', $d' = 7.78$.

Therefore

$$Re = 7.78(\frac{d}{L})^{0.145}(GrPr)^{0.356} \quad (A\text{-}5)$$

APPENDIX C-2 Regression of data using a two parameter model

The experimental data obtained from runs 1 to 30 were regressed according to the model

$$\ell n(Re) = a + b\{\ell n(GrPr) - \overline{\ell n(GrPr)}\} \quad (A\text{-}6)$$

using a linear least square regression program.

From experimental data, $\overline{\ell n(GrPr)} = 19.176$.

Results obtained with regression showed that:

$a = 8.555$, and $b = 0.387$.

Now equation (A-6) can also be written in the following form as:

$$\ell n(Re) - \ell n(c) = b\ \ell n(GrPr) \qquad \text{(A-7)}$$

where

$$\ell n(c) = a - b\ \overline{\ell n(GrPr)} \qquad \text{(A-8)}$$

or

$$Re = c\ (GrPr)^{b} \quad . \qquad \text{(A-9)}$$

With the above values for a and b, $c = 3.12$.

Therefore

$$Re = 3.12\ (GrPr)^{0.387} \quad . \qquad \text{(A-10)}$$

APPENDIX C-3 Test for the significance of the term $(\frac{d}{L})$

The significance of the additional term $(\frac{d}{L})$ was tested by examining the extra sum of square due to it.

With the two parameter model of Equation (A-6), the residual sum of square RSS1 = 1.145 with (n-2) degrees of freedom where n=30.

With the three parameter model of Equation (A-1), the residual sum of square RSS2 = 1.098 with (n-3) degrees of freedom where n=30.

The extra sum of square due to the additional term = (RSS1-RSS2) with (3-2) degrees of freedom.

Now

$$\frac{(RSS1-RSS2)/(3-2)}{(RSS2)/(n-3)} \sim F(3-2,n-3)$$

The calculated value for the term on the left hand side was equal to 1.163; F(1,27) at 95% confidence level is equal to 4.21; therefore, since $1.163<F(1,27)$, the additional term of $(\frac{d}{L})$ is insignificant.

APPENDIX D PHYSICAL PROPERTIES

APPENDIX D-1 Physical Properties of Water Used in the Theoretical Analysis

Physical properties of water from Kreith[23] were expressed in the following linear forms for use in the computer program.

(i) Density

$$\rho = 71.482 - 1.706 \times 10^{-2} \times T \qquad (lb/ft^3)$$

(ii) Heat Capacity

$$C_p = 0.978 + 3.529 \times 10^{-5} \times T \qquad (BTU/lb/^oF)$$

(iii) Thermal Conductivity

$$k = 0.165 + 3.529 \times 10^{-4} \times T \qquad (BTU/Hr/ft/^oF)$$

(iv) Absolute Viscosity

$$\mu = 2.229 \times 10^{-3} - 3.118 \times 10^{-6} \times T \qquad (lb/ft/sec)$$

Note that T is in Degree Rankin and the above equations are valid for the temperature range from 90 to 175 Degree Fahrenheit.

APPENDIX D-2 Physical Properties of Water Used for the Experimental Data Analysis

The density, viscosity, Prandtl number and the buoyancy factor for water were obtained from the same source as above and plotted as functions of temperature in Figures A-5 to A-8.

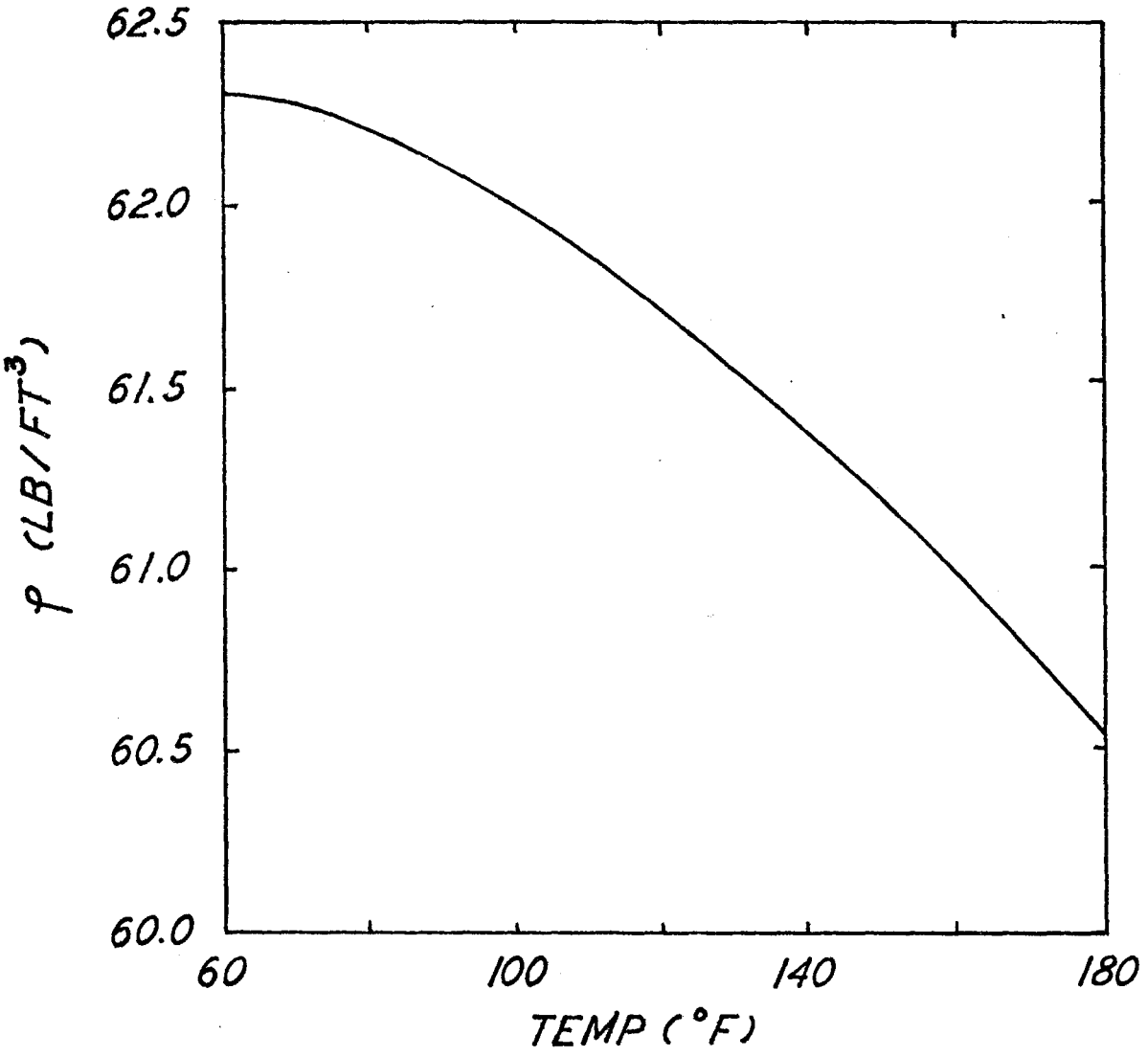

Figure A-5 Density of Water

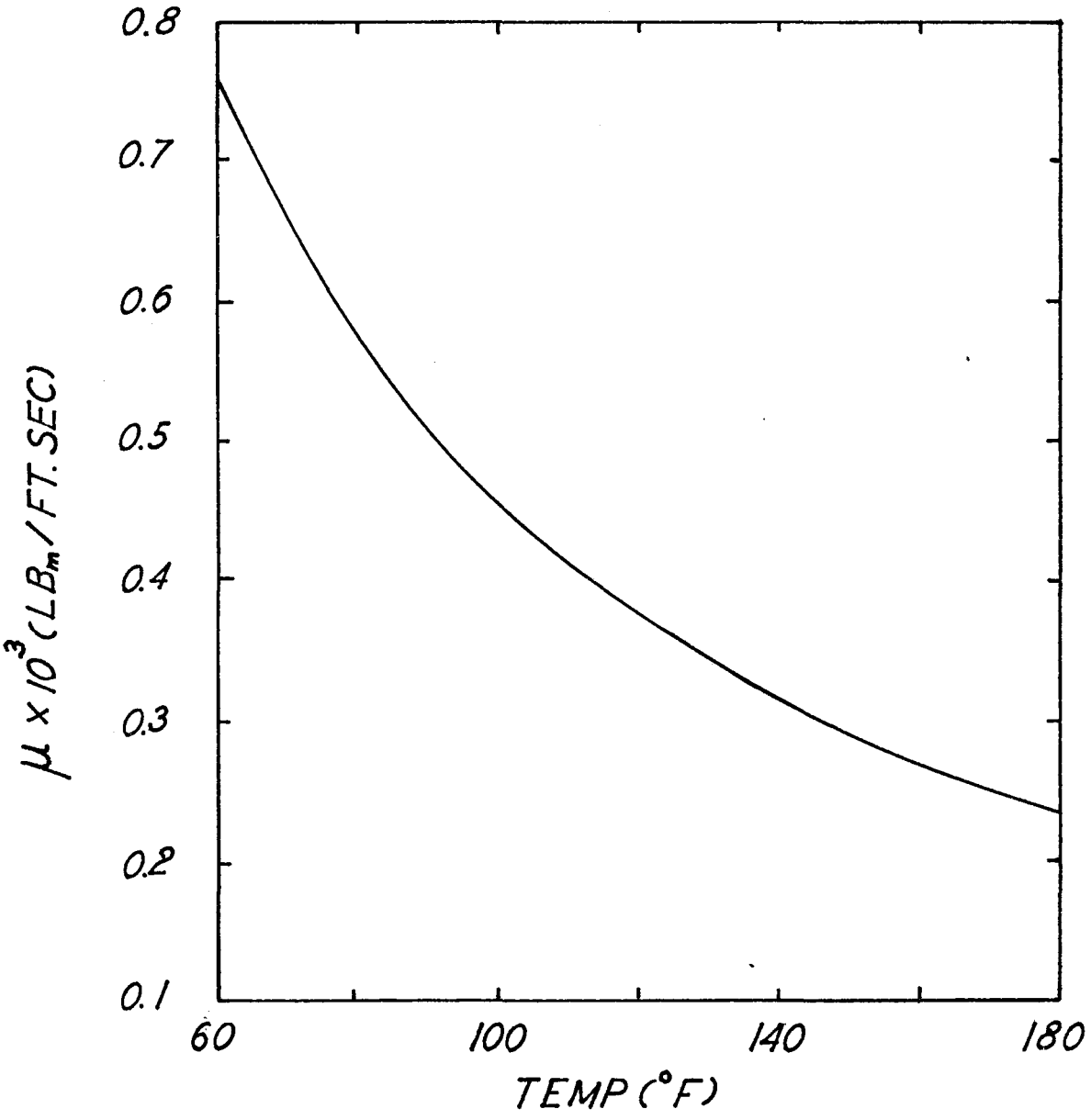

Figure A-6 Viscosity of Water

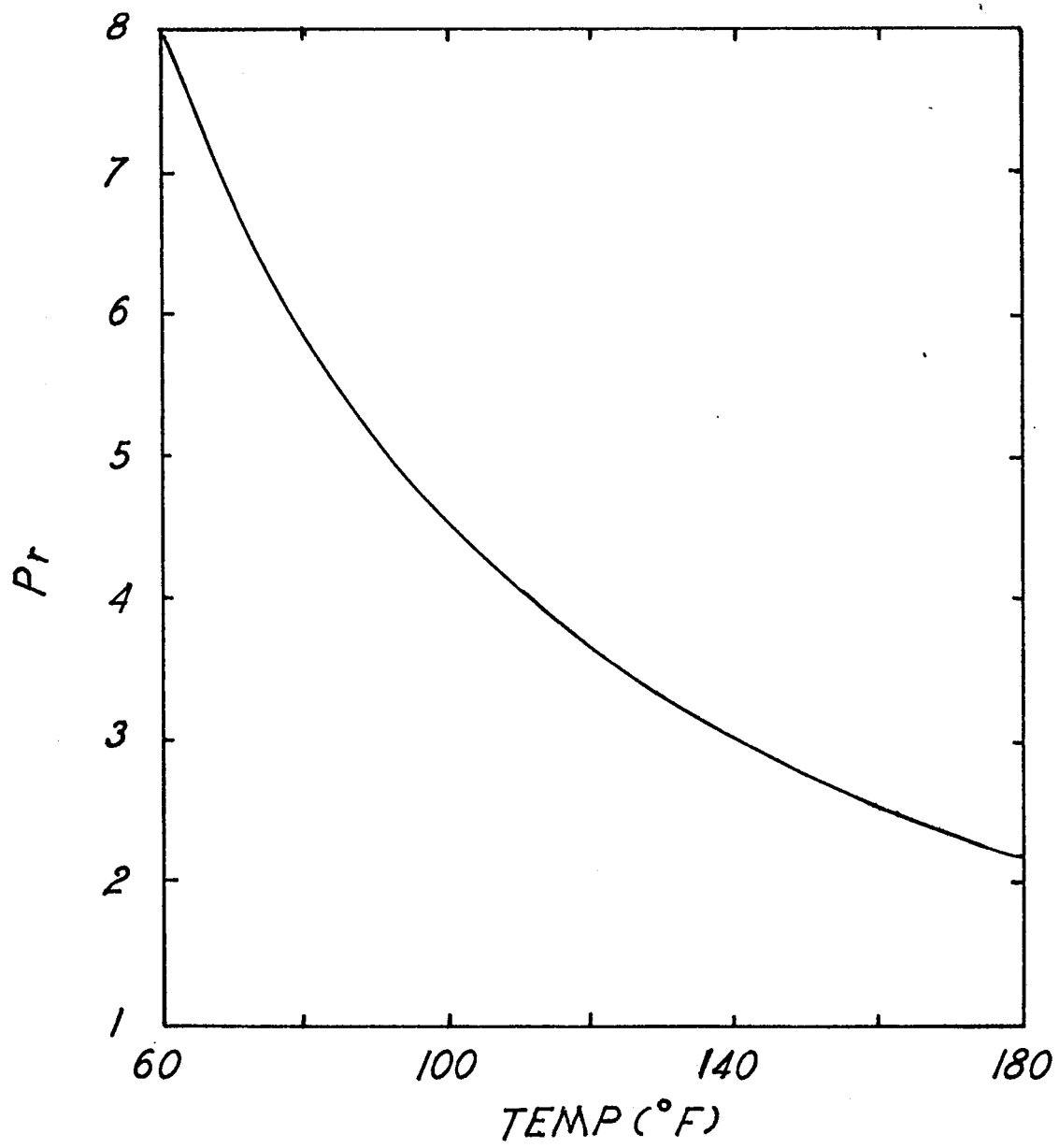

Figure A-7 Prandtl Number for Water

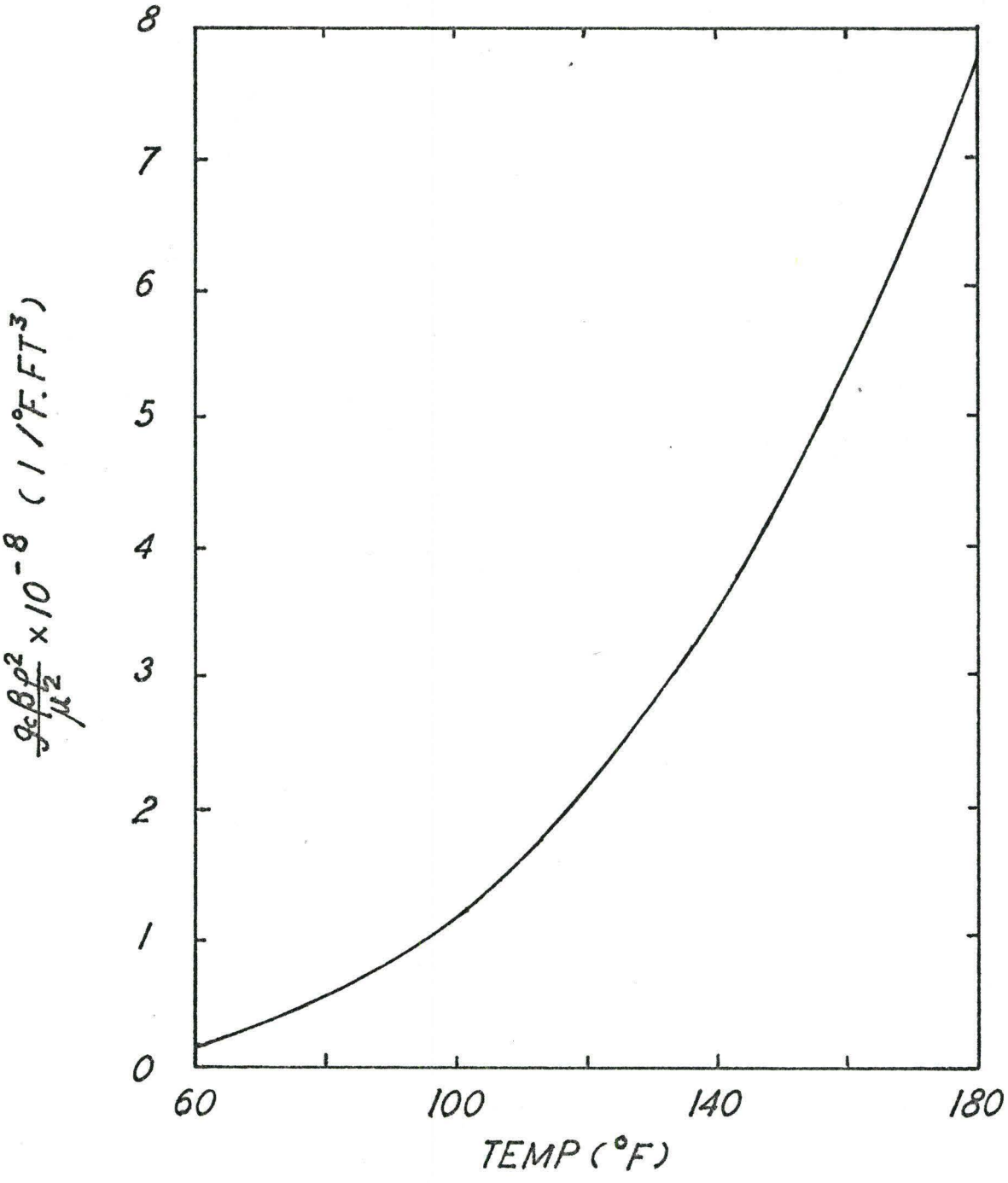

Figure A-8 Buoyancy Factor for Water

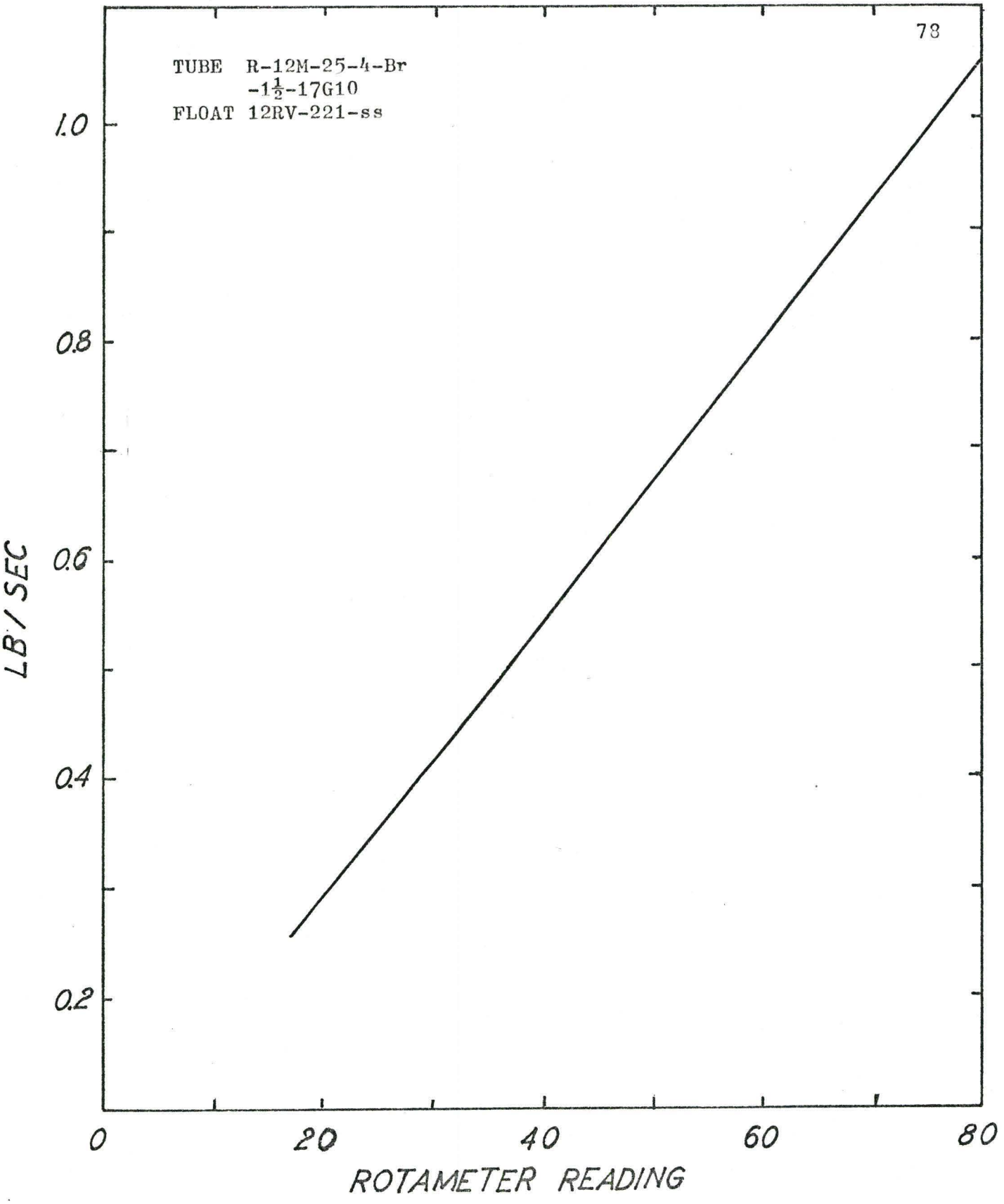

Figure A-9 Calibration of Rotameter used for the 3in. and 4in. Test Sections

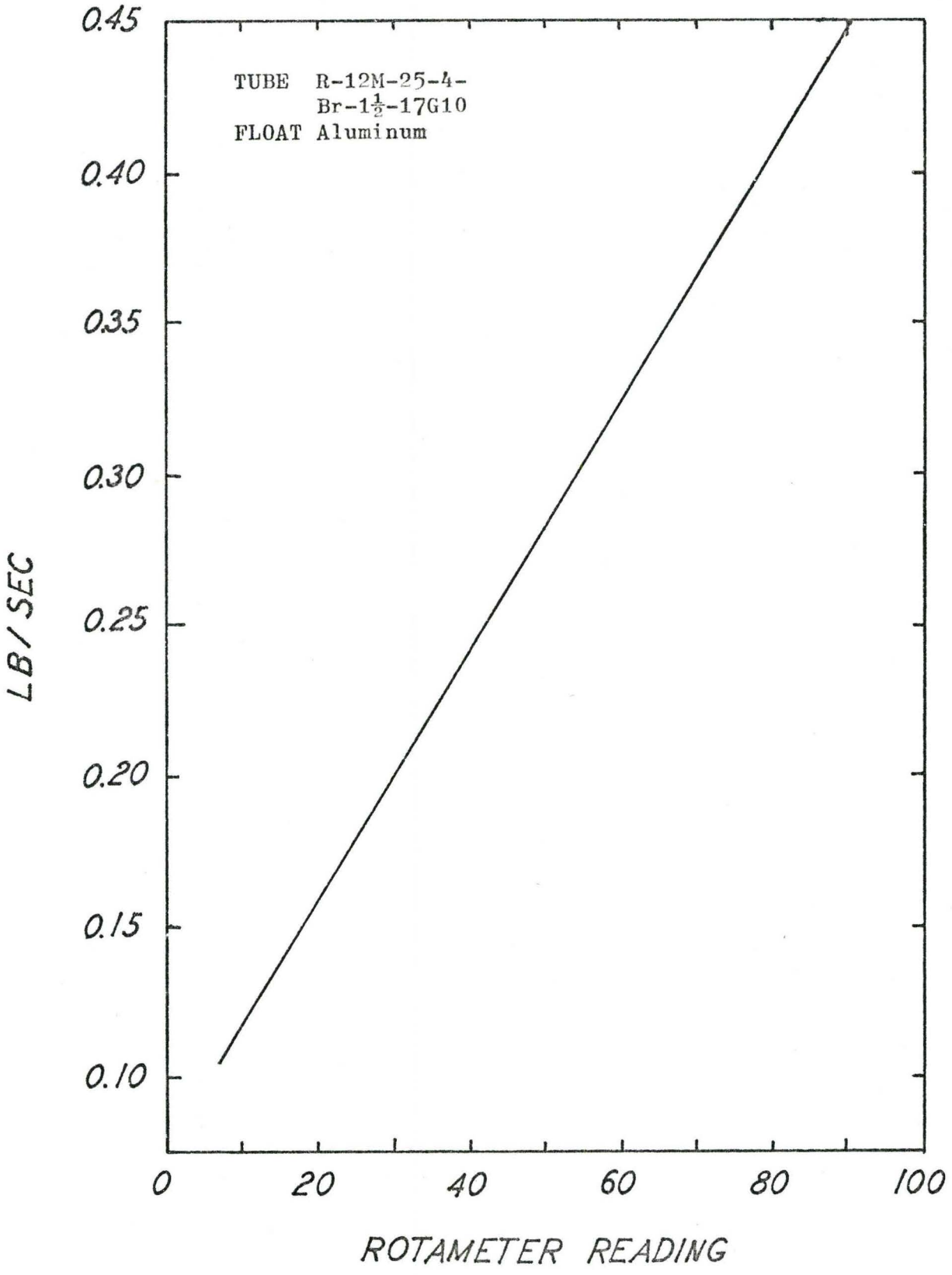

Figure A-10 Calibration of Rotameter Used for the 2 in. Test Sections

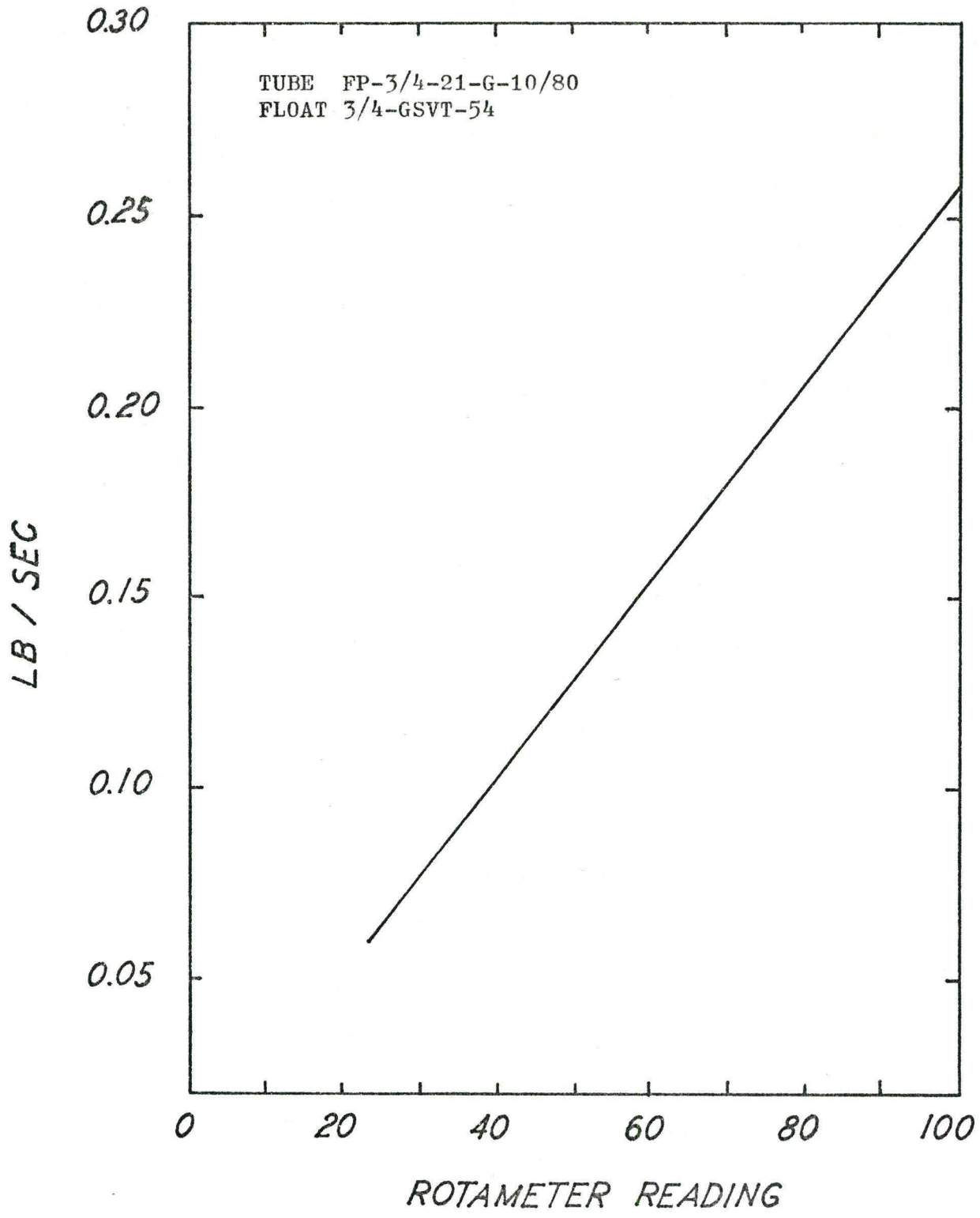

Figure A-11 Calibration of Rotameter Used for the 1-1/4 in. Test Section

THYMOL BLUE (Na SALT)

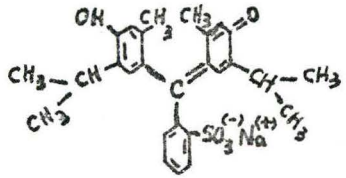

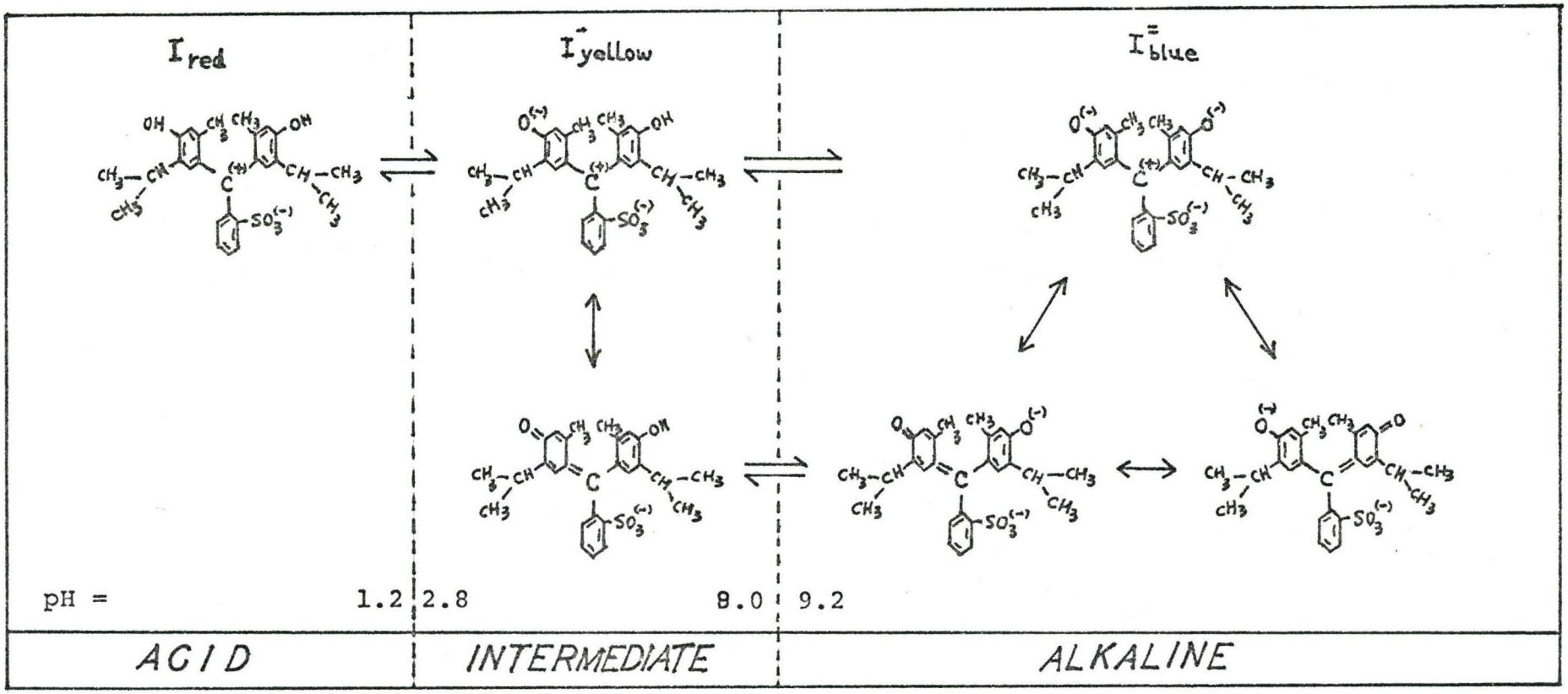

Fig A-12 STRUCTURAL CHANGES OF THYMOL BLUE Ref (24)